IEEE Access
Multidisciplinary | Rapid Review | Open Access Journal

Received 31 October 2022, accepted 30 November 2022, date of publication 6 December 2022,
date of current version 12 December 2022.

Digital Object Identifier 10.1109/ACCESS.2022.3227034

RESEARCH ARTICLE

Dual Polarized, Multiband Four-Port Decagon Shaped Flexible MIMO Antenna for Next Generation Wireless Applications

JAYSHRI KULKARNI[1], (Senior Member, IEEE), ABDULLAH G. ALHARBI[2], (Member, IEEE), CHOW-YEN-DESMOND SIM[3], (Senior Member, IEEE), ISSA ELFERGANI[4,5], (Senior Member, IEEE), JAUME ANGUERA[6], (Fellow, IEEE), CHEMSEDDINE ZEBIRI[7], (Senior Member, IEEE), AND JONATHAN RODRIGUEZ[4], (Senior Member, IEEE)

[1]Department of Electrical and Computer Engineering, Baylor University, Waco, TX 76706, USA
[2]Department of Electrical Engineering, Faculty of Engineering, Jouf University, Sakaka 42421, Saudi Arabia
[3]Department of Electrical Engineering, Feng Chia University, Taichung 407 102, Taiwan
[4]Instituto de Telecomunicações, Campus Universitário de Santiago, 3810-193 Aveiro, Portugal
[5]School of Engineering and Informatics, University of Bradford, BD7 1DP Bradford, U.K.
[6]Department of Electronics and Telecommunication Engineering, Universitat Ramon Llull, 08022 Barcelona, Spain
[7]Laboratoire d'Electronique de Puissance et Commande Industrielle (LEPCI), Department of Electronics, University of Ferhat Abbas, Sétif 19000, Algeria

Corresponding author: Issa Elfergani (i.t.e.elfergani@av.it.pt)

This work was supported in part by the European Union's Horizon 2020 Research and Innovation Program under Grant H2020-MSCA-RISE-2018-EXPLOR-872897, in part by the Fundação para a Ciência e a Tecnologia (FCT)/MEC through national funds and when applicable co-financed by the European Regional Development Fund (ERDF) under Grant PT2020, and in part by the Partnership Agreement under Project UID/EEA/50008/2020.

ABSTRACT A compact, dual polarized, multiband four-port flexible Multiple Input Multiple Output (MIMO) antennae with the connected ground and high isolation is designed with computation and experimental measurement studies. All four monopole radiators are embedded decagon-shaped flexible FR-4 substrate with an outer radius of 10 mm in order to accomplish circularly polarized (CP) radiations, bandwidth enhancement, and compact size of only $45\times38\times0.2$ mm^3 ($0.375\lambda\times0.316\lambda\times0.0016\lambda$, at lowest resonating frequency 2.5GHz). The interconnected ground structure is loaded with an Interlaced Lozenge Structure (ILS) to suppress the surface wave radiations resulting in low mutual coupling between the radiators. The proposed MIMO antenna demonstrates measured 10-dB impedance bandwidths of 9.63% (2.37–2.61 GHz), 28.79% (3.30–4.41 GHz), and 16.91% (4.98–5.90 GHz) in the LTE 38/40, Sub-6 GHz 5G NR n77/n78, WLAN and Wi-Fi bands, respectively. Furthermore, broad 3-dB Axial Ratio Bandwidth (ARBW) of 28.79% (3.30–4.41 GHz) with gain greater than 4 dBi and efficiency above 80% are achieved. Finally, the bending analysis of the proposed flexible MIMO antenna along the X- and Y- directions shows good performances in terms of scattering parameters, 3 dB ARBW, and MIMO diversity parameters.

INDEX TERMS ARBW, dual polarized, flexible, LTE, MIMO, sub-6 GHz 5G NR, Wi-Fi, WLAN.

I. INTRODUCTION

The Quality of Service (QoS) of wireless communication can be characterized in terms of high data rate, broad bandwidth, low latency, and reliability for indoor and outdoor applications. The MIMO antennas (incorporating multiple transmitting and receiving antennas) are gaining considerable attention in WLAN applications as they enhance the channel capacity and data rate without surrendering extra spectrum or transmitted power in a rich multipath fading environment.

Therefore, to enhance the transmission capacity and mitigate the multipath fading effect, the technique of deploying MIMO antennas in a restricted space is a preferred solution. The MIMO antennas design with various geometries (with or

The associate editor coordinating the review of this manuscript and approving it for publication was Bilal Khawaja.

without decoupling structures) are reported in [1] and [5], and amid these designs, [1] has reported a two-port MIMO antenna design with space diversity functions, while [2], [5] has implemented a four-port multiband MIMO antenna to enhance the channel capacity. Even though the works in [2] and [5] can cover the 5G NR n77/n78, they are of linearly polarized (LP) senses, and due to polarization mismatch as well as uncorrelated fading multipath, the receiving antennas may achieve an unequal power amplitude that affects the diversity gain (DG) and signal-to-noise ratio (SNR). Notably, the polarization mismatch effect can be minimized by employing a CP MIMO antenna, instead of an LP MIMO antenna. Because MIMO antenna with CP radiation can further mitigate multipath effects, it can therefore improve the channel capacity and QoS.

To generate CP MIMO/diversity radiations for C-band, 5G sub-6 GHz, WLAN, and K-band (for satellite applications), several two-port [6], [13] and four-port [14], [17] MIMO antennas designed with different approaches such as modifying the patch structure, the use of offset feeding line, and slot-loading in the ground plane have been reported. In [6], a corner-truncated square patch of size $56 \times 32 \times 3$ mm^3 was reported to generate a desirable CP bandwidth (or 3-dB ARBW) of 15.3% (5.08–5.92 GHz) with a 10-dB impedance bandwidth of 21% (5.12–6.32 GHz). In [7], a dual port, dual polarized MIMO antenna ($150 \times 100 \times 0.8$mm^3) with two radiators and good isolation has been reported with an operating band of (2.47–2.55 GHz). A dual-polarized MIMO antenna with pattern diversity designed-body communication is reported in [8]. The reported design has applied two stubs extended from the left and right ground plane to generate a desirable CP radiation with 100% overlapping of 10-dB impedance bandwidth and 3-dB ARBW of 19.13% (5.2–6.3 GHz). In [9], a dual-polarized CP MIMO antenna was achieved by using a branch line coupler and dual-feed probes to excite a stacked square patch (with multilayer structure and vias) for the K band applications. Nevertheless, the antennas in [6] and [9] are designed using an expensive Roger substrate that substantially increases the manufacturing cost of dual-polarized due to the manufacturing cost of building a two-port MIMO antenna, many antenna engineers have relied on a typical low-cost substrate, known as the FR-4 [10], [13]. In [10], a dual-polarized two-port planar slot MIMO antenna fabricated on a low-cost FR-4 substrate with Split Ring Resonators (SRR) as an isolating element for C-band applications has been reported. In this case, the antenna dimension is $105 \times 50 \times 1.6$mm^3, and to yield a desirable 3-dB ARBW of 8.97% (4.245–4.635) GHz, a rectangular slot is loaded into the ground plane, followed by introducing a perturbed T-shaped ground stub into the slot. A coplanar waveguide (CPW) fed wideband two-port CP MIMO antenna with a pie-shaped decoupled structure is introduced in [11] and occupies an area of 100×70 mm^2. In dual-polarized CP MIMO antenna with a lined patch to reduce the mutual coupling between the adjacent antenna elements has been introduced with broad 10-dB impedance bandwidth of 36% and 3-dB ARBW of 23% across the bands of interest. However, the MIMO antenna units do not share a common ground plane, and hence, they may not be suitable for practical realization when integrated into a compact-size wireless device. By further observing the CP MIMO antenna design in [10] and [12], they have exhibited very large dimensions that may restrict the feasibility of integrating into a low-profile wireless device. Therefore, a compact size (97×27.69 mm^2) two-port CP MIMO antenna for 5.8 GHz WLAN applications is reported in [13], and good CP radiation is achieved by loading a dual-slot 90° apart on a truncated corner rectangular patch. Even though [13] has reduced size, it has also exhibited narrow 10-dB bandwidth and 3-dB ARBW of 1.5% (5.77–5.86 GHz), which limits its application in many modern wireless devices. Nevertheless, the implementation of a 2-port MIMO antenna design configuration is not a desirable solution for accommodating a much greater number of users, and thus the development of compact-size MIMO antenna types (especially those with CP radiation) is presently the research hotspot in the area of Wi-Fi MIMO antenna design.

Recently, many different types of CP MIMO antenna design structures have been introduced [14], [17]. Amid these designs, [14] has introduced a 4×4 pentagonal microstrip element CP MIMO antenna with a size of $186 \times 188 \times 1.6$ mm^3. In [15], a dual CP stacked patch antenna based on a reflector for a 4×4 MIMO configuration operating at a 2.4 GHz WLAN band is investigated However, due to the use of two stacked FR-4 substrates (each has a thickness of 1.53 mm), it has a very large overall antenna size of $157 \times 96 \times 39$ mm^3 which limits its feasibility of integrating into a low-profile wireless device. To reduce the antenna size to $60 \times 60 \times 1.6$ mm^3, a wideband four-port CP MIMO antenna composed of four G-shaped monopole radiators with decoupling structure is investigated in [16]. The antenna operates in the Sub-6 GHz band and an I-shaped feeding strip is utilized to generate CP radiation with 3-dB ARBW of 6.70% (3.46–3.7 GHz). A dual CP MIMO antenna comprising of four G-shaped monopole elements, in which two CP elements are left-hand CP and the other two are right-hand CP are reported in [17]. To achieve a very wide 3-dB ARBW of 67.7% (4.2–8.5 GHz) with good isolation of $>$ 18dB between any two adjacent CP elements, a cross-shaped decoupling structure was applied to interconnect the ground plane of each CP element, but at the cost of increasing the overall size of this MIMO antenna to $70 \times 68 \times 1.6$ mm^3.

Apart from the above CP MIMO antenna design, dielectric resonator (DR) based antennas have also been studied as they can yield a much wider CP bandwidth [18], [23]. Amid these designs, desirable CP radiations are generated by applying the following techniques, such as the L-type feeding network [18], 45° truncation of diagonally placed DR element [19] for 5G applications, Y-shaped DR [20] for WLAN and WiMAX, offset feeding and asymmetrical cut [21] for 5 GHz WLAN, alignment of DR material with zero distance [22] for (7.72–8.08 GHz), and parasitic patch with DR element [23] for WiMAX applications. However, it is notable that the

DR-based antennas are bulky in construction and exhibit a high profile due to the thickness of DR material.

An antenna that is built on a flexible substrate [24], [28] can aid in reducing the overall antenna dimension (especially the profile) as well as the ability to bend the antenna for specific unique applications (such as wearable devices), therefore, it is imperative to study further the performances of antennas using a flexible substrate. Similar to the antenna design that has applied rigid substrate, flexible antenna design can also be applied to many wireless applications, such as the UWB [25], MIMO wearable [26], [27], and MIMO reconfigurable type [28]. However, the above reported flexible antennas are two-port LP antennas with undesirable isolation levels between the antenna elements.

In view of the above investigation, this research work has proposed a novel, compact, multiband, and flexible four-port dual-polarized antenna for wireless application.

II. GEOMETRY AND LAYOUT OF SINGLE DECAGON-SHAPED FLEXIBLE MONOPOLE ANTENNA

The top and breakdown views of a single decagon-shaped flexible monopole antenna are illustrated in Figures 1a to 1c. The antenna element is printed on a flexible, cost-effective and decagon shaped FR-4 substrate (relative permittivity $\epsilon_r = 4.4$, loss tangent tan $\delta = 0.025$, thickness h = 0.2 mm) with physical dimensions of $20\times19\times0.2\text{mm}^3$ ($0.166\lambda\times0.158\lambda\times0.001\lambda$, at 2.5 GHz).

The equations (1) and (2) [29] can be applied for determining the radius of decagon substrate at medium resonating frequency f_r (3.6GHz), using c as speed of light (3×108 m/s).

$$a_e = a\left\{1+\frac{2h}{\pi a\varepsilon_r}(ln\frac{\pi a}{2h})+1.7726\right\}^{\frac{1}{2}} \quad (1)$$

In the above equation, ''a'' is expressed as in equation (2) and ''ae'' is an effective radius of the decagon FR-4 substrate.

$$a = \frac{1.8421c}{2\pi f_r\sqrt{\varepsilon_r}} \quad (2)$$

By solving equations (1) and (2) and using optimization technique in 3-D electromagnetic Computer Simulation Technology Microwave Studio Suit (CST MWS), a_e is achieved as 10 mm for better performance of antenna elements and compactness. For this corresponding radius of 10 mm, the optimized side length of the decagon FR-4 substrate is 6.18 mm.

As mentioned earlier, the proposed monopole antenna is composed of a U-shaped radiator with a middle-protruded diamond-shaped ring radiator top-loaded by a horizontal strip. Due to the decagon-shaped substrate, the two ground planes used to support the coplanar waveguide (CPW) fed technique with beveled corners. Here, a 50Ω CPW-fed microstrip transmission line with length L_b and width W_c is sandwiched between the two beveled corners ground planes, leaving an air gap width of W_a on both sides to achieve good impedance matching. A commercially available

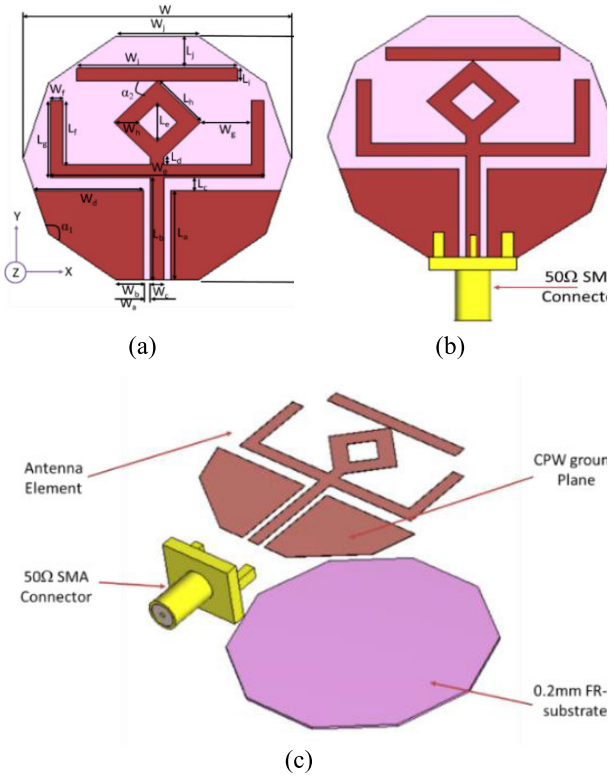

FIGURE 1. Geometry of the proposed single decagon-shaped flexible monopole antenna.

SMA connector (Type 10) is utilized in this case, and it is also included during the simulation process, as depicted in Figures 1b and 1c. Notably, the two ground planes are beveled at an interior angle of $\alpha_1 = 144°$ without disturbing the SMA connector to achieve good CP radiations across the desired operating band.

At the top of the microstrip transmission line, a U-shaped radiator of equal arm length L_g and width W_f is loaded to generate a resonance at 2.5 GHz. The air gap L_c between the U-shaped radiator and ground planes reduces the inductive impedance by producing an equal amount of capacitive reactance, thus achieving good impedance matching at 2.5 GHz, and it is maintained throughout the desired operating band. To further induce a second resonance at 3.6 GHz, a diamond-shaped ring radiator with side length L_h and ring-corner width W_h protruded from the middle section of the U-shaped radiator via a short connecting strip of length L_d. By further observing Figure 1, one can also see that the two corners of the diamond-shaped ring radiator have an air gap distance of W_g away from the two vertical arms of the U-shaped radiator. Here, the middle square slot used to form the diamond-shaped ring radiator has a slot size of $L_e\times L_e$ for improving the impedance matching at 3.6 GHz. Finally, to generate a third resonance at 5.5 GHz, a horizontal strip of length W_i and width L_i is affixed at the top of the diamond-shaped radiator at an angle of α_2. The angle α_2 and horizontal strip result in bandwidth enhancement by producing a longer path for surface current at resonating frequency of 5.5 GHz.

TABLE 1. Design parameters details and their optimized dimensions of the proposed monopole antenna.

Single Antenna			
Parameters	**Value (mm)**	**Parameters**	**Value (mm)**
W	20	L	19
W_a	0.5	L_a	7
W_b	2.1	L_b	8
W_c	1.5	L_c	10.95
W_d	8.2	L_d	0.6
W_e	16	L_e	3
W_f	1	L_f	5
W_g	5	L_g	6
W_h	1.7	L_h	3.82
W_i	12	L_i	1.5
W_j	6.21	L_j	4
α_1	144°	α_2	45°
MIMO Antenna		**Decoupling structure**	
Parameters	**Value (mm)**	**parameters**	**Value (mm)**
WW	45	W_m	3.6
LL	38	W_n	0.8
W_k	9.04	L_m	3.6
W_l	18.79	L_n	1.6
L_k	10.95	L_o	7
L_l	9	-	-
α_3	72°	-	-

The optimized parameters of the designed antenna are listed in Table 1.

A. WORKING MECHANISM OF THE PROPOSED DECAGON-SHAPED FLEXIBLE MONOPOLE ANTENNA

The stepwise design stages of the proposed decagon-shaped flexible monopole antenna with five different layouts are depicted in Figure 2, and their corresponding reflection coefficient (S_{11}) and (AR) dB diagrams are illustrated in Figure 3. As shown in Figure 2a, the U-shaped radiator designed in Step-1 induces a resonance at 2.5 GHz (as defined in Figure 3), and it is printed on a square-shaped flexible substrate. The length of the U-shaped radiator ($2L_g+W_e$) is a quarter-wavelength long at a resonance frequency of 2.5 GHz. In Step 1, due to the CPW-fed technique applied to the U-shaped radiator, excellent impedance matching is achieved, and it can produce a 10-dB impedance bandwidth of 0.24 GHz (2.38–2.62 GHz) covering the LTE 38/40, as shown in Figure 3a. However, as seen in Figure 3b, the AR values are around 40 dB, so the antenna in Step-1 is an LP radiator. In Step-2, as shown in Figure 2b, a diamond-shaped radiator protrudes from the U-shaped radiator to induce a resonance at 3.6 GHz without disturbing the antenna defined in Step-1. As the air gap distance of W_g reduces the inductive reactance (produced due to the addition of a diamond-shaped radiator), it maintains the impedance matching at 3.6 GHz. Hence, Step-2 can successfully resonate at 3.6 GHz with an impedance bandwidth of 0.82 GHz (3.40–4.22 GHz) covering a partial 5G Sub-6 GHz band n77/n78. To further enhance the antenna's bandwidth introduced in Step-2, a diamond slot is loaded into the diamond-shaped radiator,

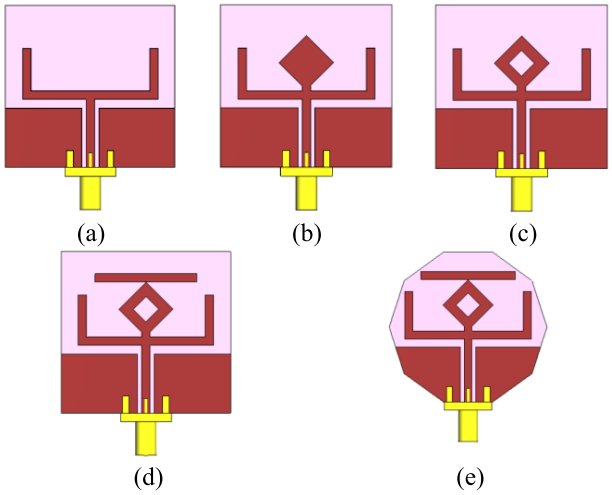

FIGURE 2. Stepwise design of proposed decagon shaped flexible antenna (a) Step-1, (b) Step-2, (c) Step-3 (d) Step-4, (e) Step-5.

forming a diamond-shaped ring radiator that produces a higher-order mode of 4.44 GHz, as shown in Figure 2c. As this higher-order mode has overlapped with the fundamental mode at 3.6 GHz, the antenna in Step-3 can now yield wider impedance bandwidth of 1.14 GHz (3.30–4.44 GHz) covering the 5G Sub-6 GHz band n77/78, as shown in Figure 3a. The horizontal symmetricity of the diamond-shaped ring structure perturbs the current distribution on the radiator and generates the two electric vector field components, namely, E_x and E_y with equal amplitude (across 3.30–4.18 GHz) frequency band, as shown in Step-2 and Step-3 of Figure 3b (with AR $<$ 3 dB).

To achieve resonance at 5.5 GHz further, in Step-4, a horizontal strip whose length is a quarter-wave long at 5.5 GHz is loaded onto the top-corner section of the diamond-shaped ring radiator in Step-3, as shown in Figure 2d. Here, the antenna in Step-4 can yield 10-dB impedance bandwidth of 0.75 GHz (5.20–5.95 GHz) with LP radiations (AR $>$ 30 dB), as shown in Figures 3a and 3b, respectively, and it cannot cover the 5.2 GHz, WLAN band. To further enhance the impedance bandwidth at a higher frequency and to increase the E_x and E_y electric field vectors with equal amplitude (0 dB or $\sim$1) and phase difference ($\Delta\emptyset = \pi/2$) across (3.30–4.44 GHz), Step-5 is developed, as shown in Figure 2e, in which the entire flexible substrate was reduced to a decagon shape (from a square-shaped type), and the two CPW-fed ground planes are now with a beveled corner. This transformation enhances the impedance bandwidth of the proposed monopole (Step-5) to 0.91 GHz (5.02–5.93 GHz) with LP radiations covering the WLAN/Wi-Fi 5 and enhances the CP radiations (3.30–4.44) across the Sub-6 GHz band n77/78, as shown in Figures 3a and 3b, respectively.

B. SURFACE CURRENT DISTRIBUTION OF THE PROPOSED DECAGON-SHAPED FLEXIBLE MONOPOLE ANTENNA

Figures 4a, 4b, and 4c analyses the surface current distributions of the proposed monopole antenna element excited

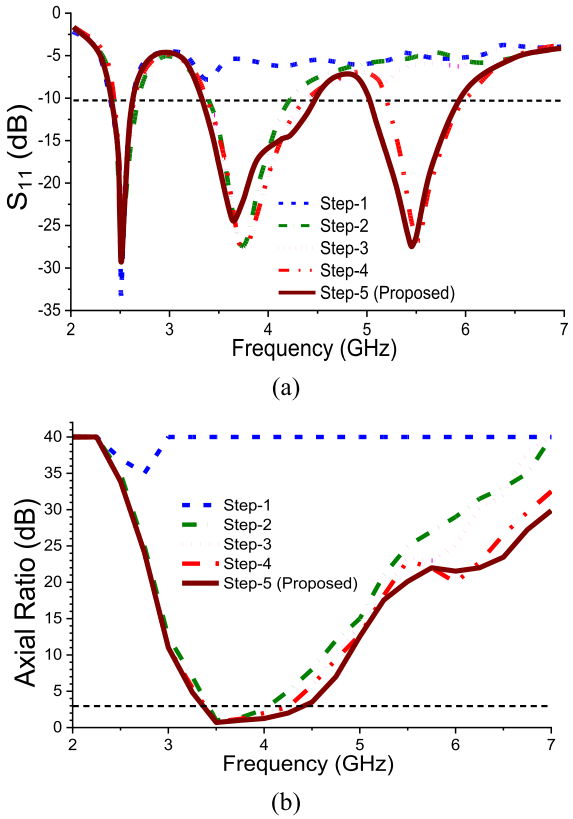

FIGURE 3. Stepwise results of proposed decagon-shaped flexible antenna (a) S_{11} (dB) (b) AR (dB).

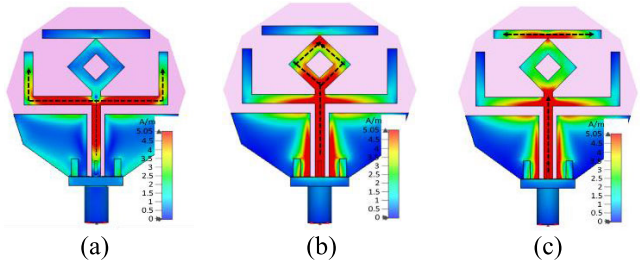

FIGURE 4. Surface current distributions of the proposed decagon-shaped flexible monopole antenna at various frequency, (a) f_L = 2.5 GHz, (b) f_M = 3.6 GHz, and (c) f_H = 5.5 GHz.

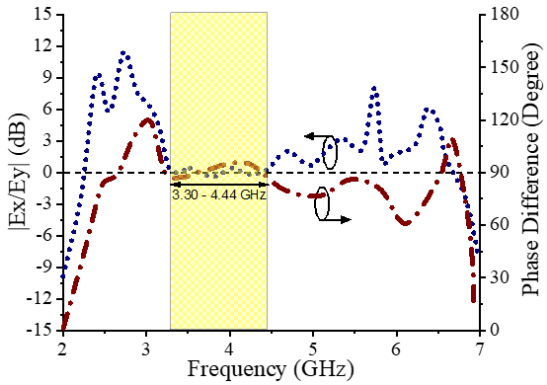

FIGURE 5. Amplitude ratio and phase difference of the proposed decagon-shaped flexible monopole antenna.

at the low band (f_L) 2.5 GHz, middle band (f_M) 3.6 GHz, and high band (f_H) 5.5 GHz, respectively. In Figure 4a, the U-shaped radiator has exhibited a half-wavelength current distribution path at f_L, with an operating band of (2.38–2.62 GHz). As shown in Figure 4b, a quarter-wavelength current distribution path f_M is also demonstrated along with the diamond-shaped ring radiator, resulting in the excitation of the (3.30–4.44 GHz) band. Finally, as visualized in Figure 4c, a half-wavelength current distribution path at f_H is depicted across the top-loaded horizontal strip, showing a broad operational band of (5.02–5.93 GHz).

C. CP MECHANISM OF THE PROPOSED DECAGON-SHAPED FLEXIBLE MONOPOLE ANTENNA

To fully comprehend the CP excitation of the proposed monopole antenna element (or the antenna in Step-5) across the band of interest (3.30–4.44 GHz), Figure 5 depicts its corresponding calculated amplitude ratio (E_x/E_y) and PD of the two orthogonal electric field components. Here, one can observe that the amplitude ratio is closer to 0 dB with PD of near 90° across the band of interest.

The surface current distribution of the antenna in Step-5 is analyzed from Figures 6a to 6d at f_M for the variation of phase angle at 0°, 90°, 180°, and 270°, respectively. Initially, at the 0° phase, the maximum current vectors are in the +y direction, whereas at the 180° phase, the current flows in the -y direction. The current vectors are equal in amount and flow in the opposite direction at 90° and 270° phases. Thus, the current vectors are changing with time (in a counter-clockwise manner) that illustrating the RHCP radiations of the antenna evaluated in Step-5 (proposed monopole antenna element).

III. BENDING ANALYSIS OF THE PROPOSED DECAGON SHAPED FLEXIBLE MONOPOLE ANTENNA

To investigate the effects of bending the proposed monopole antenna, its corresponding simulated S_{11}, gain, and efficiency curves are analyzed and shown in Figures 7 and 8. A complete cylindrical Styrofoam with $\varepsilon_r = 1.03$ and a radius of 15 mm is utilized to bend the flexible antenna along the X- and Y-direction, as shown in Figures 7 and 8. Here, the bending of the proposed monopole antenna along the X-axis and Y-axis has demonstrated a very small effect (minor frequency shift) across the f_L (2.5 GHz), f_M (3.6 GHz), and f_H (5.5 GHz) operating bands.

IV. DESIGN OF THE FOUR-PORT DECAGON SHAPED DUAL-POLARIZED FLEXIBLE MIMO ANTENNA WITH ILS

The geometry and breakdown view of the proposed four-port decagon-shaped dual-polarized flexible MIMO antenna is shown in Figures 9a and 9b, respectively. The proposed MIMO antenna is composed of four identical decagon-shaped monopole radiators arranged in a mirror image fashion with each other, as portrayed in Figure 9.

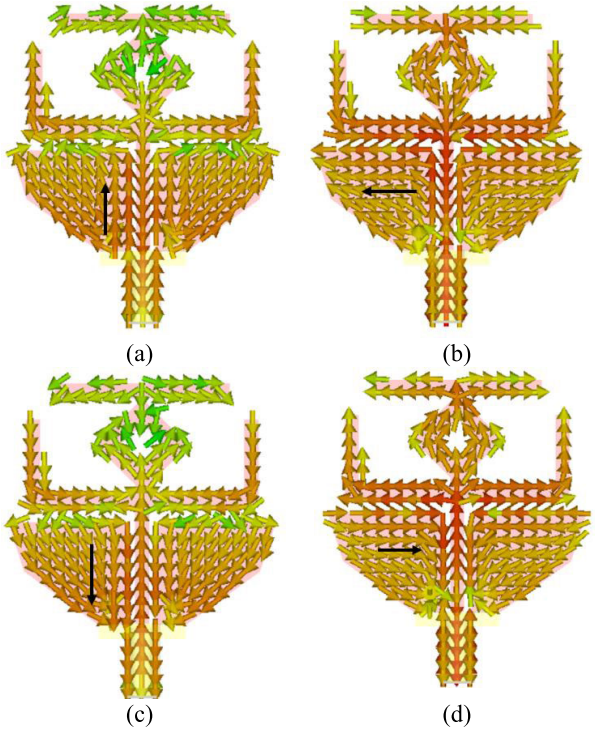

FIGURE 6. Surface current distributions at f_M (3.6 GHz) with different phases, (a) 0°, (b) 90°, (c) 180°, (d) 270°.

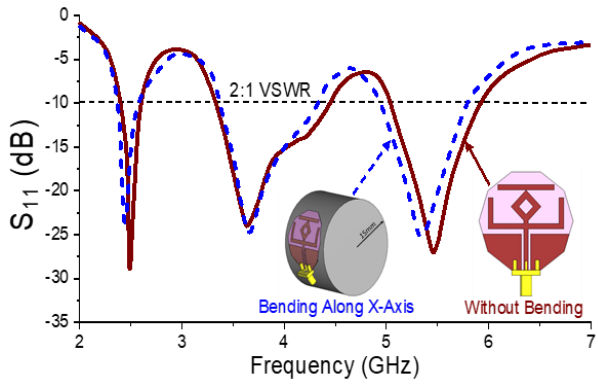

FIGURE 7. Effects on the S_{11} when bending the proposed decagon-shaped flexible monopole antenna along the X-axis.

The antenna radiators are arranged such that the Ant. 1 and Ant. 2 are separated by a distance of W_o, whereas the Ant. 1 and Ant. 4 are separated by an edge-to-edge distance of L_p. A trapezium-shaped patch is utilized to interconnect the disconnected ground planes between Ant. 1 and Ant. 2, as well as between Ant. 3 and Ant. 4. Here, a decoupling structure (ILS) has been deployed in the antenna elements' interconnected ground planes to suppress the radiating waves and obtain high isolation among adjacent antenna elements. The hexagon-shaped slot formed in the middle of the flexible FR-4 substrate further minimized the mutual coupling between Ant.1 and Ant. 4, as well as between Ant. 2 and Ant. 3. The mirrored pattern of the monopole radiators supports the polarization diversity in the respective operative

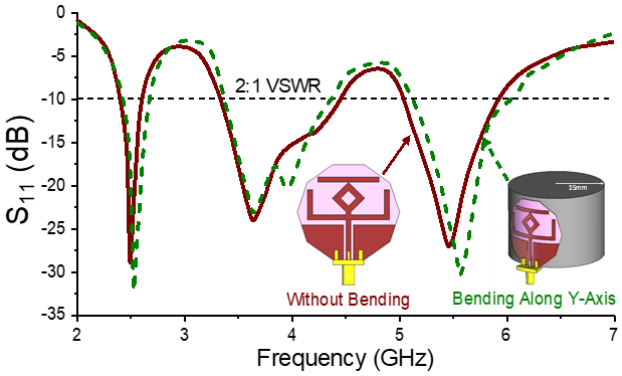

FIGURE 8. Effects on the S_{11} when bending the proposed decagon-shaped flexible monopole antenna bending along the Y-axis.

bands. Therefore, Ant. 1 and Ant. 3 induce RHCP radiations, whereas LHCP radiations are excited across the Sub-6 GHz frequency band. The four-port MIMO antenna is designed on a flexible FR-4 substrate of 0.2 mm thick with an occupied area of 45×38 mm^2. The parameters of the proposed dual-CP MIMO antenna are also listed in Table 1.

A. DESIGN PROCESS OF THE PROPOSED FOUR-PORT DECAGON SHAPED DUAL POLARIZED FLEXIBLE MIMO ANTENNA

The evolution steps of the proposed MIMO antenna are illustrated in Figures 10a-c. The main aim is to obtain a wide 3 dB ARBW with interconnected ground planes of antenna elements. Initially, four monopole radiators are deployed in a mirror image pattern, as shown in Figure 10a. Here, Ant. 2 is a mirror image of Ant. 1, whereas Ant. 3 and Ant. 4 are mirror images of Ant. 2 and Ant. 1, respectively. For any MIMO antenna, the incurred mutual coupling can be minimized by leaving sufficient space (spatial diversity) among the radiators. Hence, proper spacing is arranged between the radiators to preserve a good 3 dB ARWB of the individual antenna element. However, this results in a disconnected ground plane between Ant. 1 and Ant. 2, as well as between Ant. 3 and Ant. 4. The S_{11}, S_{12}, and AR of this configuration are shown in Figures 11a-c (Blue dashed line). It is observed that there are negligible effects on S_{11} and AR, and good isolation larger than 20 dB is also achieved. However, for practical realization, the ground planes of the four antenna elements must be interconnected. Therefore, a trapezium-shaped patch is loaded between Ant. 1 and Ant. 2, as well as between Ant. 3 and Ant. 4, so as to interconnect the ground planes, as shown in Figure 10b. From Figures 11a-c (green dashed line), it is observed that the 3 dB ARBW and mutual coupling between antenna elements degrade significantly. However, it is a fact well-known that it is quite challenging to preserve a wide ARBW of the antenna elements and to maintain good isolation when the antenna elements are closely deployed in a restricted space with interconnected ground planes. To improve the isolation between adjacent antenna elements, an ILS (decoupling structure) [31], [35] is loaded

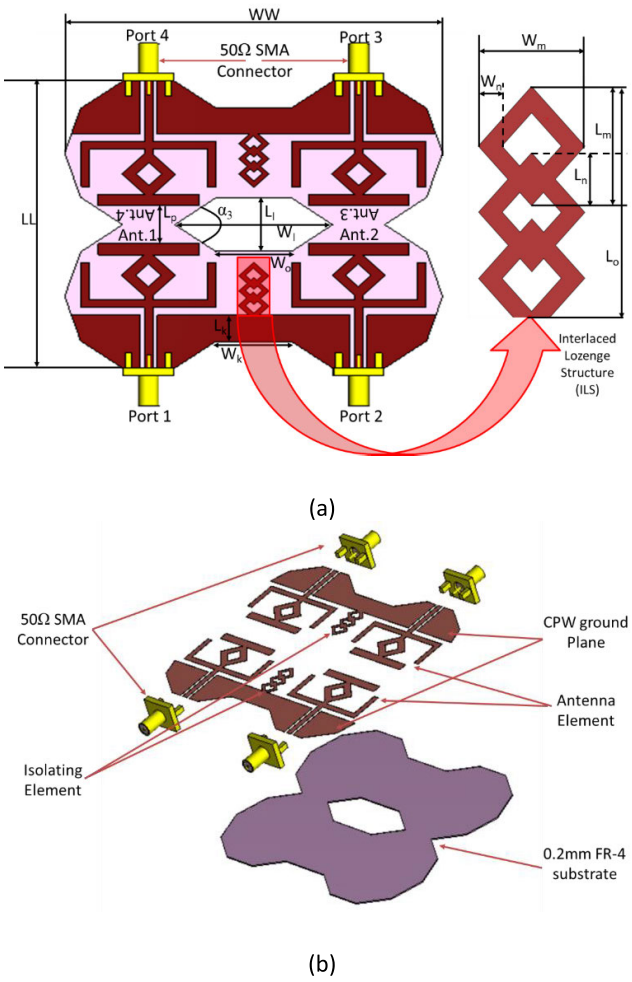

FIGURE 9. Geometry of the proposed decagon-shaped flexible MIMO antenna, (a) Front view, and (b) Breakdown view.

between the antenna elements, as displayed in Figure 10c. The proper location of the ILS is anticipated in such a way that the minimal coupling between the antenna elements and wide 3 dB ARBW can be preserved. With the addition of ILS, the ARBW of the designed antenna element increases significantly. It is clearly noted from Figures 11a-c (Brown line) that the ILS has a negligible effect on the 10-dB impedance bandwidth but considerably enhances the isolation between the antenna elements and the 3 dB ARBW.

To further verify the design steps of the proposed decagon-shaped dual polarized flexible MIMO antenna, the surface current distributions when only port-1 is activated are depicted in Figures 12a-c. It is easily noted from Figure 12a that Ant. 1 and Ant. 2 are not mutually coupled with each other due to disconnected ground resulting in suppressing the radiating waves from Ant. 1, whereas, in Figure 12b, Ant. 1 and Ant. 2 are strongly coupled with each other due to coupled ground and Ant. 2 is getting affected by the electric field of Ant. 1 resulting in co-related signals in a rich multipath fading environment. As seen from Figure 12c, after the loading of ILS, it is able to suppress the radiating

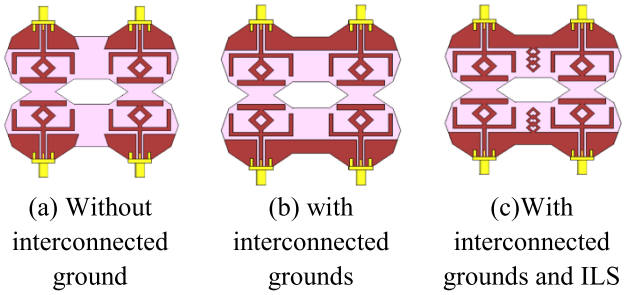

FIGURE 10. Evaluation process of the proposed decagon-shaped dual polarized flexible MIMO antenna.

wave from Ant. 1 and protect Ant. 2 from the influence of the electric field of Ant. 1. This results in achieving un-correlated signals between Ant. 1 and Ant. 2 and reduction of mutual coupling between antenna elements. The same is also valid for Ant. 3 and Ant. 4.

B. POLARIZATION DIVERSITY OF THE PROPOSED FLEXIBLE FOUR-PORT MIMO ANTENNA

The surface current distributions (A/m) are further considered to realize the dual CP mechanism of the proposed MIMO antenna. Figures 13a-d analyze the surface current distributions for the variation of the phase angle at 0°, 90°, 180°, and 270° at f_M (3.6 GHz) when all four ports are excited simultaneously. The maximum current vectors at Ant. 1 and Ant. 2 are in the +Y direction at the 0° phase, whereas at the 180° phase, the maximum current vectors of Ant. 1 and Ant. 2 are in the -Y direction. At 90° and 270° phases, the surface current vector distribution of Ant. 1 and Ant. 2 are equal in amplitude and flow opposite in phases. Equivalently, at 0° phase, the maximum current vectors of Ant. 3 and Ant. 4 flow in the -Y direction, while at the 180° phase, the current distribution vectors of Ant. 3 and Ant. 4 flow in the +Y direction. The current distributions of Ant. 3 and Ant. 4 are equal in amplitude flows with opposite phase angles. As a result, as displayed in Figure 13d, the current vectors of Ant. 1 and Ant. 3 are changing with time and rotating in an anti-clockwise direction, demonstrating the RHCP mechanism of Ant. 1 and Ant. 3. Likewise, the current vector distributions of Ant. 2 and Ant. 4 change with time and rotate in a clockwise manner, illustrating the LHCP mechanism of Ant. 2 and Ant. 4.

V. RESULTS AND DISCUSSION OF THE PROPOSED DECAGON-SHAPED DUAL POLARIZED FLEXIBLE MIMO ANTENNA

To validate the proposed design, the proposed decagon-shaped dual polarized flexible MIMO antenna (loaded with two ILS) was fabricated as shown in Figure 14(a) and its radiation performance including radiation patterns, gain and efficiency were measured in anechoic chamber as shown in Figure 14(b). The simulated and measured results are well agreed with each other except for minimal deviation that may be due to fabrication error or soldering tolerances.

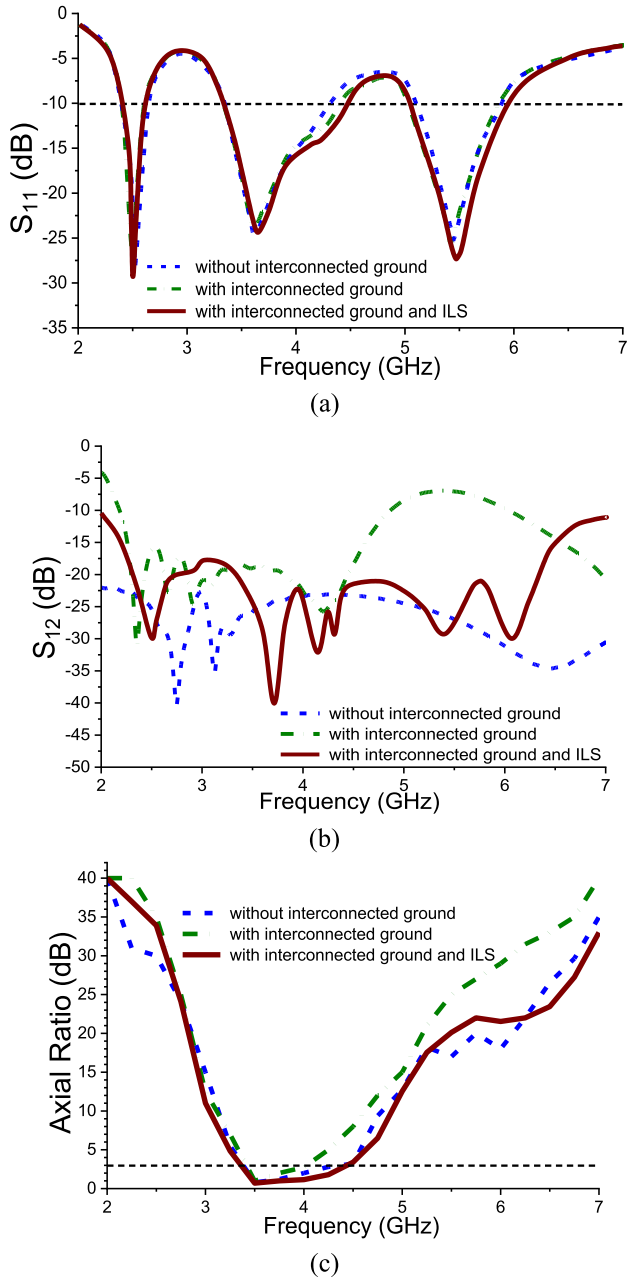

FIGURE 11. Evaluation process results of proposed decagon-shaped dual polarized flexible MIMO antenna (a) S_{11} (b) S_{12} (c) Axial Ratio.

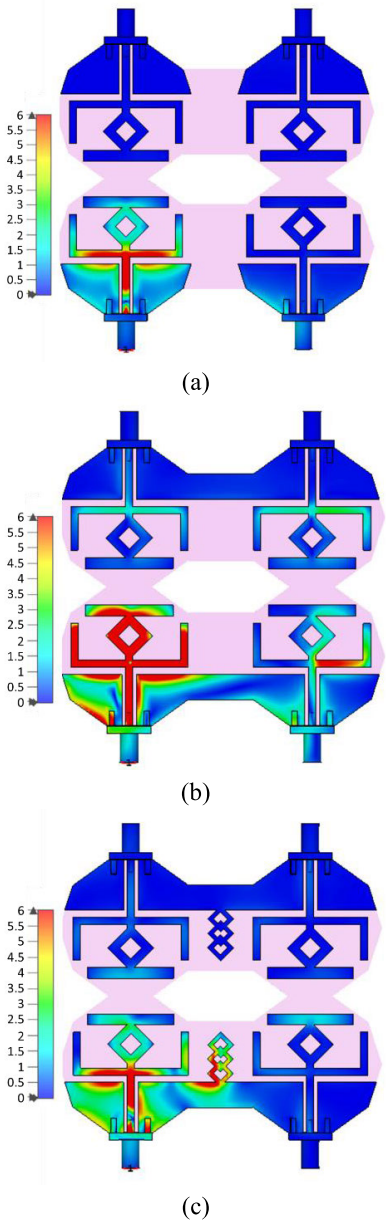

FIGURE 12. Surface current distribution of evaluation process results of proposed MIMO antenna.

A. SIMULATED AND MEASURED REFLECTION COEFFICIENT

As shown in Figure 15, the simulated 10-dB impedance bandwidths of the proposed MIMO antenna across the three bands of interest were $f_L = 9.18\%$ (2.39–2.62 GHz), $f_M = 29.45\%$ (3.30–4.44 GHz), and $f_H = 16.62\%$ (5.02–5.93 GHz). Their corresponding measured 10-dB impedance bandwidths were 9.63% (2.37–2.61 GHz), 28.79% (3.30–4.41 GHz), and 16.91% (4.98–5.90 GHz), respectively. Thus, the proposed MIMO antenna can operate across the LTE 38/40, 5G Sub-6 GHz NR band n77/n78, and WLAN band applications for next-generation wireless devices.

The equation to calculate the S- parameters in terms of reflection coefficient (S11) at three different resonating frequencies is as follows

S_{11} = magnitude of the reflection coefficient = (VSWR-1)/(VSWR+1)

The magnitude of S11 in terms of dB is expressed as follows:

$$S_{11}\,(dB) = -20log\frac{(VSWR-1)}{(VSWR+1)} \tag{3}$$

B. SIMULATED AND MEASURED TRANSMISSION COEFFICIENT

The simulated and measured transmission coefficients (S_{12}, S_{13}, S_{14}) of the proposed four-port decagon shaped dual

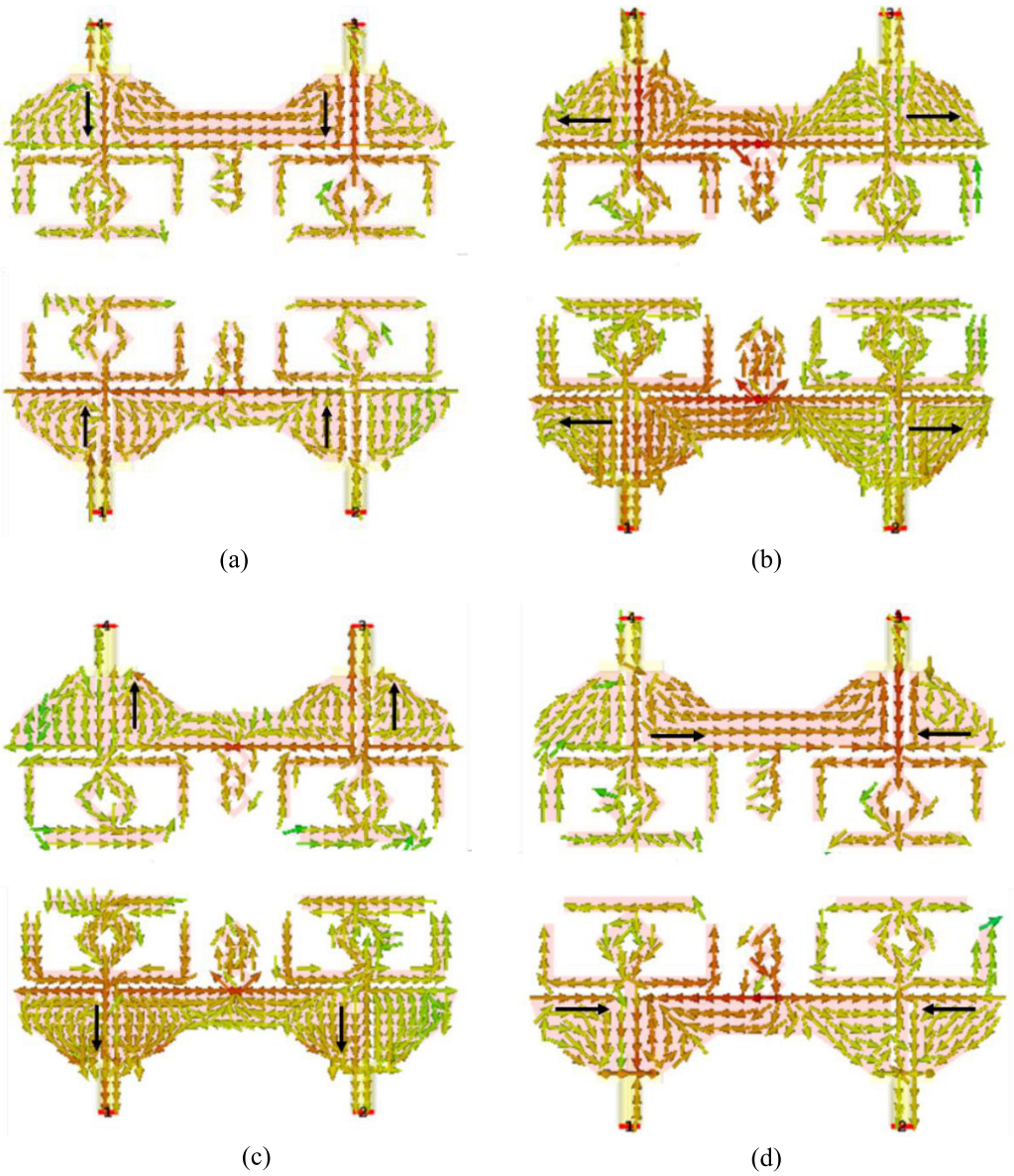

FIGURE 13. Surface current distributions of the proposed flexible MIMO antenna at f_M (3.6 GHz): (a) 0°, (b) 90°, (c) 180°, and (d) 270°.

polarized flexible MIMO antenna are displayed in Figure 16. It is very well noted that the isolation is larger than 20 dB throughout the desired bands of interest. At the time of measurement, one antenna element is active, while the remaining other antenna elements are terminated using a 50Ω load impedance.

C. SIMULATED AND MEASURED AXIAL RATIO

The simulated and measured 3 dB ARBW of the proposed decagon shaped dual polarized flexible MIMO antenna is depicted in Figure 17. It is easily visualized that the MIMO antenna possesses a very wide simulated 3 dB ARBW of 29.45% (3.30–4.44 GHz), and its corresponding measured result was 28.79% (3.30–4.41 GHz). Thus, the measured CP bandwidth can well cover the 5G Sub-6 GHz NR band n77/78 with 100% overlapping the measured 10-dB impedance bandwidth of the antenna element working in the f_M.

D. SIMULATED AND MEASURED GAIN AND EFFICIENCY

The simulated and measured gain and efficiency curves of the proposed decagon shaped dual polarized flexible MIMO antenna are depicted in Figure 18. The measured gain was above 4 dBi, and the measured efficiency was well above 80% throughout the three operating bands. Notably, the measured outcomes are well-validated with the simulated results.

E. SIMULATED AND MEASURED RADIATION PATTERNS

The simulated and measured radiation patterns at f_M (3.6 GHz) in the E-plane (xy plane) and H-plane (xz plane) of the proposed decagon shaped dual polarized flexible MIMO

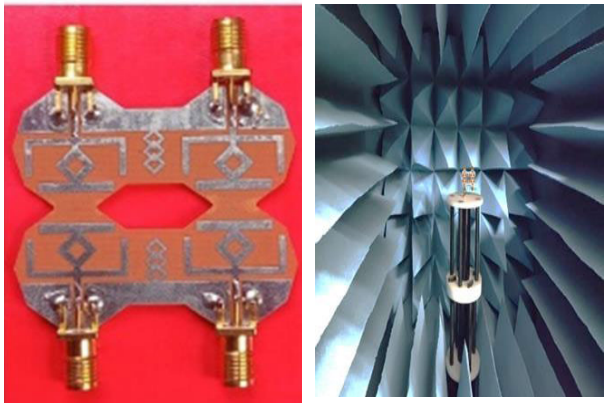

FIGURE 14. (a) Fabricated prototype of the proposed decagon-shaped dual polarized flexible MIMO antenna (b) Measurement set-up in an anechoic chamber.

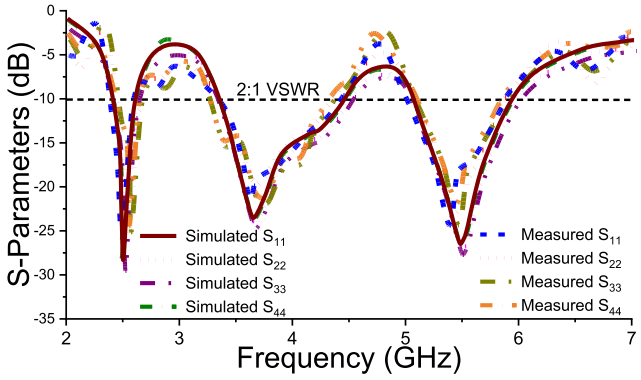

FIGURE 15. Reflection coefficient of the proposed decagon shaped dual polarized flexible MIMO antenna.

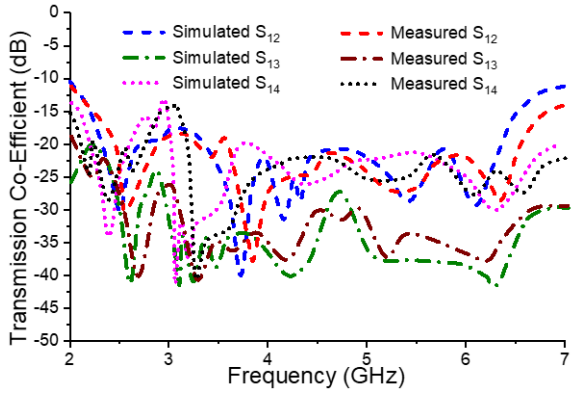

FIGURE 16. Transmission Coefficient of proposed decagon shaped dual polarized flexible MIMO antenna.

antenna are depicted in Figure 19 when all the ports are excited simultaneously. From Figure 19, it is noted that in both the planes ($\varphi = 0°$, $\varphi = 90°$), the Ant. 1 and Ant. 3 illustrate RHCP radiation patterns with 3-dB beamwidth of 78.90°±0.5 in the +z-direction. Likewise, Ant. 2 and Ant. 4 demonstrate the LHCP radiation patterns with 3-dB

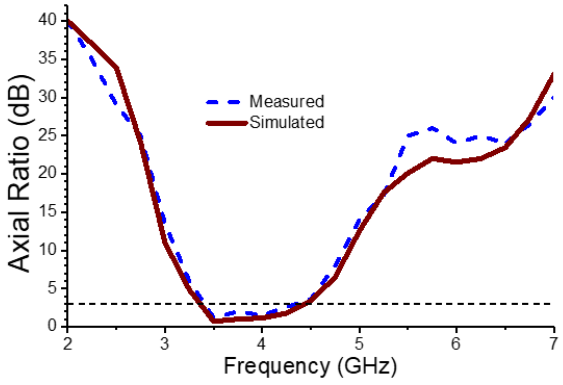

FIGURE 17. Axial ratio of proposed decagon shaped dual polarized flexible MIMO antenna.

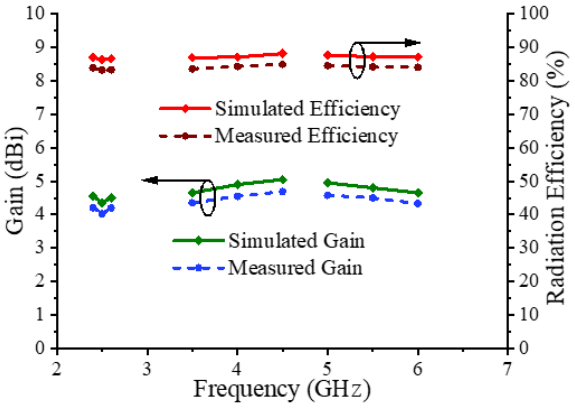

FIGURE 18. Gain and efficiency of the proposed decagon shaped dual polarized flexible MIMO antenna.

beamwidth of 79.10°±0.5 in both planes ($\varphi = 0°$, $\varphi = 90°$). Therefore, the proposed MIMO antenna generates RHCP radiations when the Ant. 1 and Ant. 3 are excited, and LHCP radiations when the Ant. 2 and Ant. 4 are excited. This validates the polarization diversity performance of the proposed decagon shaped dual polarized flexible MIMO antenna in the 5G Sub-6 GHz NR band n77/78.

The simulated and measured radiation patterns for Ant. 1, Ant. 2, Ant. 3, and Ant. 4 across the E-plane and H-plane at f_L (2.5 GHz), f_M (3.6 GHz), and f_H (5.5 GHz) are illustrated in Figure 20. It can be observed that, in E-plane, the radiation pattern of Ant. 1 and Ant. 2 are mirror images of one another (same radiation pattern in Ant. 1 and Ant. 4); similarly, Ant. 4 is the mirror image of Ant. 3 (same radiation pattern in Ant. 2 and Ant. 3). In H-plane, the radiation pattern of Ant. 1 and Ant. 4 are mirror images of one another (same radiation pattern in Ant. 1 and Ant. 2); similarly, Ant. 3 is the mirror image of Ant. 2 (same radiation pattern in Ant. 3 and Ant. 4). This proves that the proposed decagon shaped MIMO antenna has attained pattern diversity that fortifies that there is no interference during the reception and perpetuate omnidirectional radiation pattern in both E-plane and H-plane.

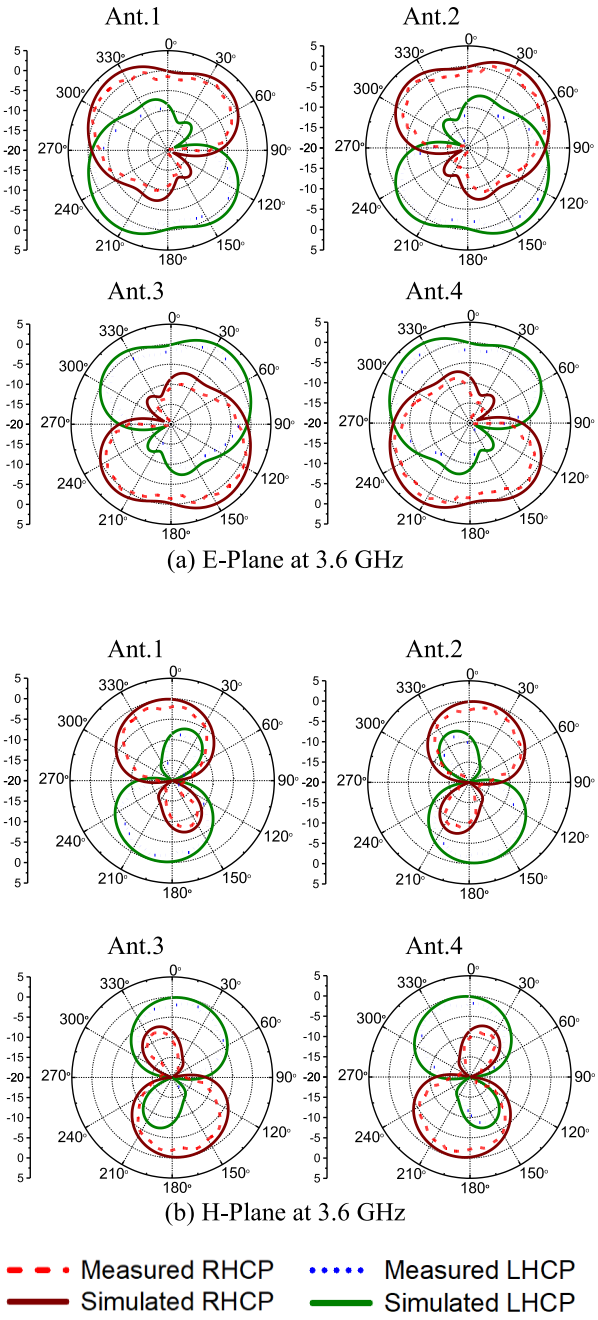

(a) E-Plane at 3.6 GHz

(b) H-Plane at 3.6 GHz

FIGURE 19. Simulated and measured circularly polarized radiation pattern at fM (3.6 GHz).

F. ENVELOPE CORRELATION COEFFICIENT (ECC) AND DIVERSITY GAIN (DG)

The envelope correlation coefficient (ECC) of the proposed decagon shaped dual polarized flexible MIMO antenna is calculated from the far-field patterns using Equation (4) as follow:

$$\rho_e = \frac{\left| \int\int \left[\overrightarrow{F_1}(\theta,\varphi) \times \overrightarrow{F_2}(\theta,\varphi) \right] d\Omega^2 \right|}{\int\int \left| \overrightarrow{F_1}(\theta,\varphi) \right|^2 d\Omega \int\int \left| \overrightarrow{F_2}(\theta,\varphi) \right|^2 d\Omega} \tag{4}$$

where '$F_i(\theta, \phi)$' is the radiated field of the ith antenna.

Figure 21 shows the ECC curves between Ant. 1-2, Ant. 1-3, and Ant. 1-4. It is observed that the calculated ECC values are less than 0.04 across the three bands of interest. Therefore, from the ECC values, it is confirmed that the proposed decagon shaped dual polarized flexible MIMO antenna has achieved high inter port isolation and better diversity performance in a rich multipath fading environment.

The diversity gain (DG) is calculated by using the below Equation (5) and it is depicted in Figure 21.

$$DG = 10\sqrt{1 - \left|\rho_{eij}\right|^2} \tag{5}$$

It is noted that the DG is very closer to 10 dB throughout the functioning bands.

G. TOTAL ACTIVE REFLECTION COEFFICIENT (TARC)

The Total Active Reflection Coefficient (TARC) between Ant. 1 and Ant. 2 is calculated using the below Equation (6), and its experimental set-up is shown in Figure 22a.

$$\Gamma = \frac{\sqrt{\left(\left|S_{ii} + S_{ij}e^{j\theta}\right|^2\right) + \left(\left|S_{ji} + S_{jj}e^{j\theta}\right|^2\right)}}{\sqrt{2}} \tag{6}$$

where θ is the input phase angle that is varied from 0^0 to 120^0 with step increment of 30^0, S_{ii} and S_{jj} are the reflection coefficients of the port i and port j, respectively. Figure 22b depicts the TARC values for polarized antenna elements, where it is visualized that under the variation of phase angle, the performances of the proposed MIMO antenna remain undisturbed in the scattering environment.

H. MEAN EFFECTIVE GAIN (MEG)

The Mean Effective Gain (MEG) is another essential parameter for the estimation of diversity performance of the proposed flexible four-port dual CP MIMO antenna.

The MEG is achieved using below Equation (7):

$$MEG_i = 0.5\mu_{irad} = 0.5\left(1 - \sum_{j=1}^{K} \left|S_{ij}\right|^2\right) \tag{7}$$

where in Equation (6), K is the number of antennas, i is the active antenna and η_{irad} is the radiation efficiency of the i^{th} antenna. Using Equations (8-11), the MEG values for Ant. 1, Ant. 2, Ant. 3, and Ant. 4 are calculated and depicted in Table 2:

$$MEG_1 = 0.5\left(1 - |S_{11}|^2 - |S_{12}|^2 - |S_{13}|^2 - |S_{14}|^2\right) \tag{8}$$

$$MEG_2 = 0.5\left(1 - |S_{21}|^2 - |S_{22}|^2 - |S_{23}|^2 - |S_{24}|^2\right) \tag{9}$$

$$MEG_3 = 0.5\left(1 - |S_{31}|^2 - |S_{32}|^2 - |S_{33}|^2 - |S_{34}|^2\right) \tag{10}$$

$$MEG_4 = 0.5\left(1 - |S_{41}|^2 - |S_{42}|^2 - |S_{43}|^2 - |S_{44}|^2\right) \tag{11}$$

From Table 2, it is confirmed that the MEG values for all four antennas are between the limit $-3 \leq$ MEG (dB) < -12 defined by industry and standards. It is also visualized that the ratio of MEG1/MEG2 and MEG3/MEG4 is approximately equal to one, which confirms that the proposed decagon

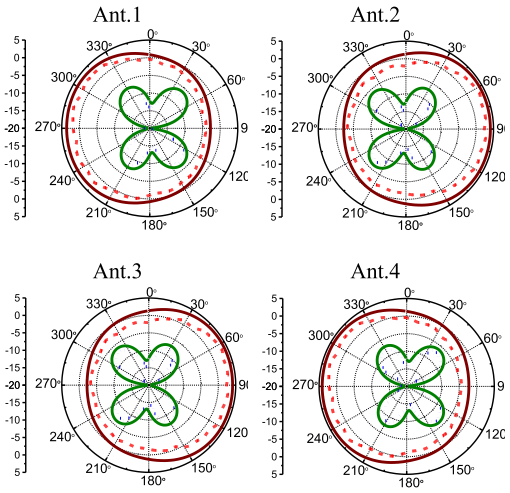

(a) E-Plane 2.5 GHz

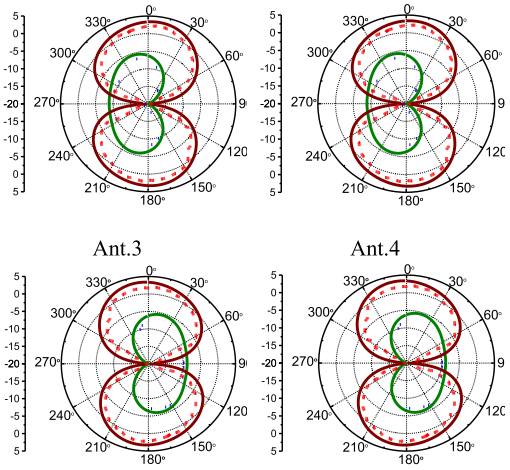

(b) H-Plane 2.5 GHz

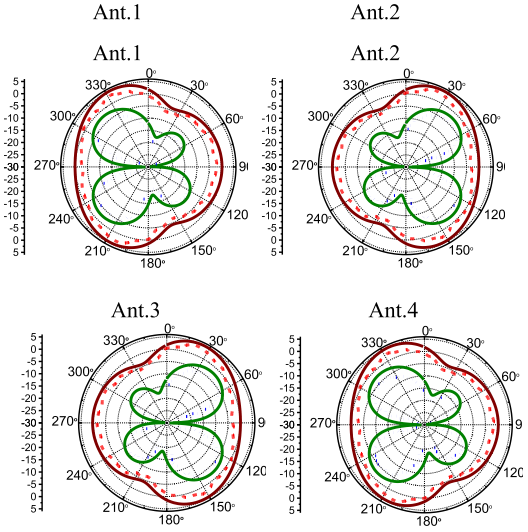

(c) E-Plane 3.6 GHz

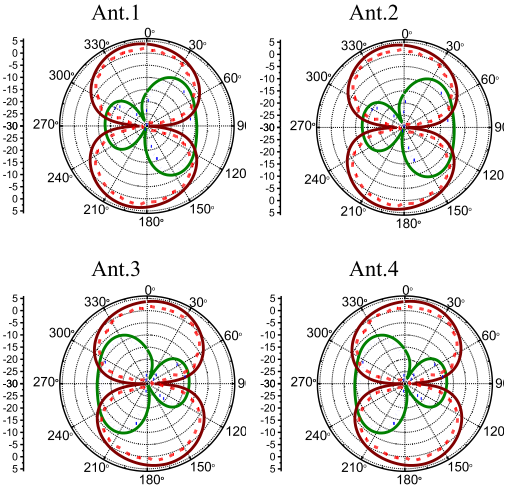

(d) H-Plane 3.6 GHz

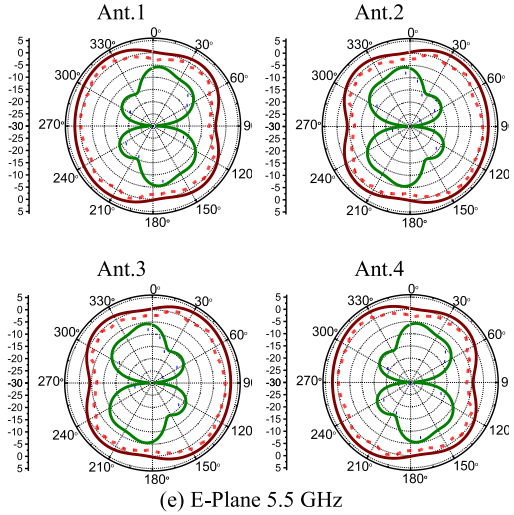

(e) E-Plane 5.5 GHz

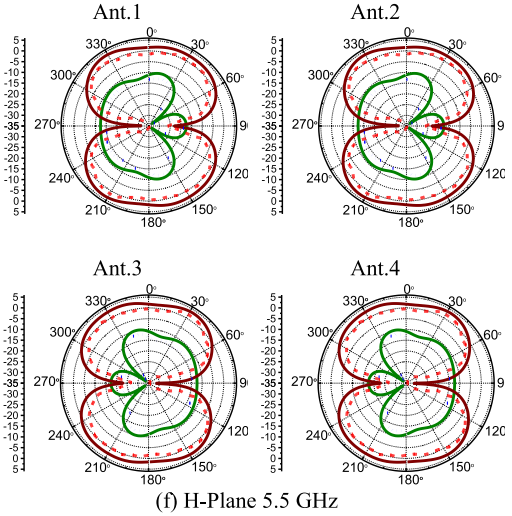

(f) H-Plane 5.5 GHz

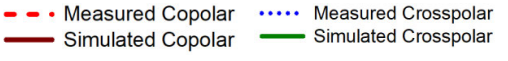

FIGURE 20. Simulated and measured linearly polarized Radiation patterns.

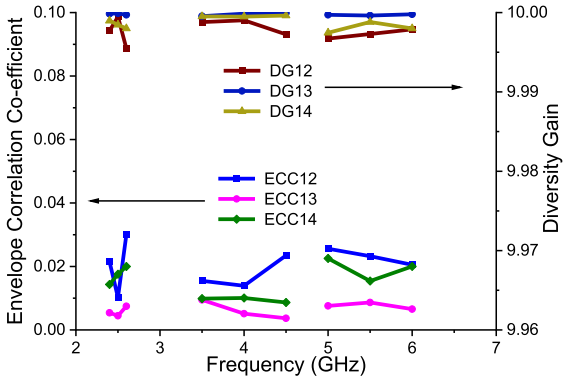

FIGURE 21. ECC and DG of proposed decagon shaped dual polarized flexible MIMO antenna.

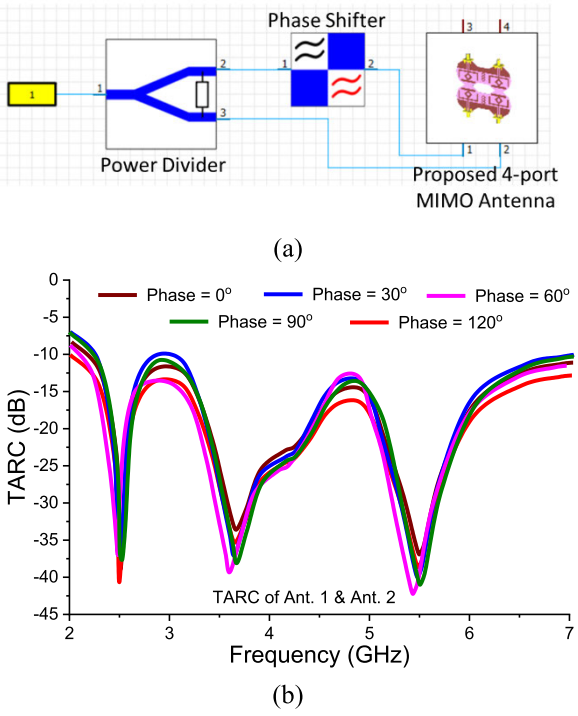

FIGURE 22. TARC of the proposed decagon shaped dual polarized flexible MIMO antenna (a) Experimental set-up (b) TARC (dB).

TABLE 2. MEG values of proposed decagon shaped dual polarized flexible MIMO antenna.

Frequency (GHz)	MEG -1 (dB)	MEG -2 (dB)	MEG -3 (dB)	MEG -4 (dB)	MEG-1/MEG -2	MEG-3/MEG -4
2.5	-4.63	-4.68	-4.75	-4.70	0.989	1.010
3.5	-4.65	-4.01	-4.09	-4.73	1.159	0.864
4.0	-4.61	-4.69	-4.73	-4.68	0.982	1.010
4.5	-4.69	-4.02	-4.98	-4.33	1.166	1.150
5.0	-4.01	-4.10	-4.61	-4.75	0.987	0.970
5.5	-4.04	-4.08	-4.09	-4.80	0.990	0.852
6.0	-4.35	-4.33	-4.53	-4.37	1.004	1.036

shape MIMO antenna system has attained better diversity performance in a multipath fading environment.

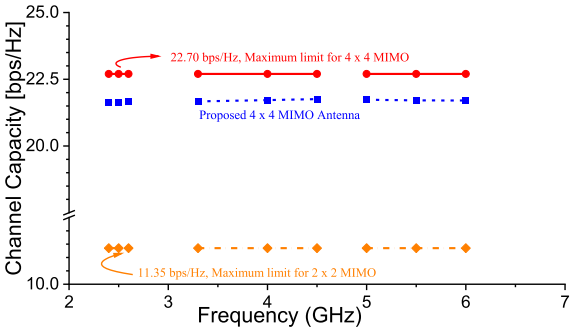

FIGURE 23. Channel capacity of the proposed decagon shaped dual polarized flexible MIMO antenna.

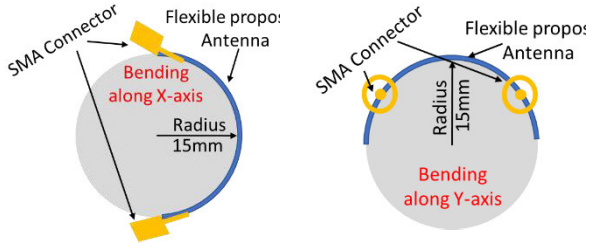

FIGURE 24. Bending analysis proposed decagon shaped dual polarized flexible MIMO antenna (a) Along X-axis (Left-side view) (b) Along Y-axis (Bottom View).

I. CHANNEL CAPACITY

The ergodic channel capacity of the proposed decagon shape dual polarized flexible MIMO antenna across the operating bands is analysed in Figure 23 using the equation mentioned in [30]. It is validated that the capacity varies between 20 and 21 bps/Hz, and it is 1.86 times greater than the maximum limit of 2 × 2 MIMO antenna.

VI. BENDING ANALYSIS OF PROPOSED FLEXIBLE FOUR PORT DUAL CP MIMO ANTENNA

To validate the bending effects of the proposed flexible MIMO antenna and make sure that it can still operate well with conformal surfaces, the effects on various typical antenna performances when bending the proposed MIMO antenna are performed unlike [36] and [38]. The simulated and fabricated bending scenarios are performed on a semi-cylindrical Styrofoam ($\varepsilon_r = 1.03$), in which the proposed flexible MIMO antenna is attached to the prescribed bending radius. Notably, the scattering parameters, AR curves, and ECC performances are considered for the validation of flexible operation by exciting port 1. Here, the proposed MIMO antenna is bent for a radius of 15 mm along the X-axis and Y-axis. The case of a 15 mm radius along both X and Y-axis is selected by assuming the worst-case scenario under the maximum bending capability of the proposed MIMO antenna as shown in Figure 24 (a) and (b).

TABLE 3. Performance comparison of proposed decagon shaped dual polarized flexible MIMO with existing state of Arts.

Ref.	No. of Ports	Size (mm^2)	Frequency (GHz)	Imp. BW (%)	ARBW (%)	Decoupling technique	CP Technique	Type of substrate	Flexible/ Non-Flexible	Gain	ECC
[5]	4	50×50	3.3 – 5.8	54.94	-	Log strips loaded on ground plane	-	FR-4	NF	> 2.5	0.01
[6]	2	56×32	5.12 – 6.32	21	15.3	Metallic plates	Truncated corner square	Taconic RF-35	NF	5.8	0.05
[7]	2	150×100	2.47 – 2.55	3.18	2.2	Ground with stubs and DGS	Offset feeding	Roger RO4350B	NF	6.1	0.003
[10]	2	105×50	3.8 – 5.4	28.52	8.97	Split ring resonators	Slot with T-shaped stub	FR-4	NF	3.60	0.16
[11]	2	177×70	4.5 – 6.5	24.23	8	Interconnected semicircles	Tilted narrow slot	FR-4	NF	5.4	0.0003
[12]	2	132×66	1.73-2.6	39.56	22	Line patch	Tapered slots	FR-4	NF	4	0.01
[13]	2	97×27.69	5.49 – 6.02	9.27	1.48	Vertical slot	Rectangular slots	FR-4	NF	5.34	0.1
[14]	4	186×188	2.36-2.53	6.95	6.95	Placing CP elements orthogonally	Truncated patch	FR-4	NF	7.95	0.002
[15]	4	157×96	2.4-2.5	7	8.1	Tapered stub and different slots	Tapered stub	FR-4	NF	8	0.02
[16]	4	60×60	3.4-3.8	11.11	11.11	Slot	strips	FR-4	NF	4.5	0.12
[18]	2	110×110	3.12 – 3.9	22.22	5.66	Spatial Diversity	Cylindrical DRA	Roger RT Duroid	NF	7.2	0.3
[21]	2	40×60	5.15-6.12	17.2	10.2	Not used	Parasitic T-shaped strip	FR-4	NF	4.5	0.3
[22]	2	80×80	5.71-8.2	34.85	4.55	Spatial Diversity	DRA	FR-4	NF	4	0.05
[26]	2	59×29	2.38-2.55	6.89	-	Parasitic strip	-	Roger	F	3.79	0.4
			3.37-3.60	6.59	-						
			4.92-5.37	8.75	-						
Proposed	4	45×38	2.37–2.61	9.63	-	ILS Structure	Beveled ground pane on decagon shaped substrate	FR-4	F	4	0.04
			3.30–4.41	28.79	28.79						
			4.98–5.90	16.91	-						

A. BENDING ANALYSIS OF PROPOSED DECAGON SHAPED DUAL POLARIZED FLEXIBLE MIMO ANTENNA ALONG X-AXIS

The proposed flexible MIMO antenna is bent from the center along the X-axis, as depicted in the simulated prototype (see Figure 25a) and the fabricated prototype (see Figure 25b). The simulated and measured S-parameter, AR, and ECC obtained after bending the MIMO antenna along the X-axis are compared with the ones without bending, as shown in Figures 25 c-e. From Figure 25c, it is visualized that there are negligible effects on the S_{11} across the f_L (2.5 GHz) and f_M (3.6 GHz), whereas a small decrease in the operational bandwidth was observed in the f_H (5.5 GHz). Notably, even though the f_H has suffered from such a decrease in the bandwidth, it still covers the entire 5 GHz WLAN band. The simulated and measured transmission coefficient of the bending MIMO antenna is well below -20 dB throughout the three operating bands, which conforms well with the simulation results without bending. From Figures 25d-e, it can be observed that there is a negligible deviation in the AR and ECC curves.

B. BENDING ANALYSIS OF THE PROPOSED DECAGON SHAPED DUAL POLARIZED FLEXIBLE MIMO ANTENNA ALONG THE Y-AXIS

The MIMO antenna is bent from the center along the Y-axis, as seen in the simulated prototype (see Figure 26a) and the fabricated prototype (see Figure 26b). The simulated and measured S-parameter, AR, and ECC obtained after bending the MIMO antenna along the Y-axis are compared with the simulated ones without bending, as shown in Figures 26 c-e. From Figure 26c, it is observed that there is a negligible effect on the bandwidth of 2.5 GHz band and 3.6 GHz band when bending the MIMO antenna, whereas a small decrease in the operational bandwidth was observed in the f_H (5.5 GHz), and the f_H is also slightly shifted towards higher spectrum. Even though the desired f_H has suffered from a

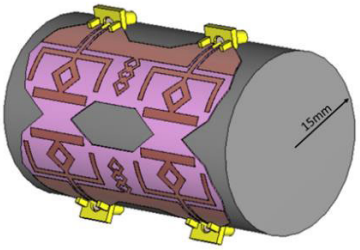

(a) Simulated Prototype

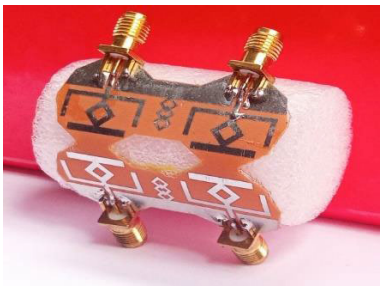

(b) Fabricated Prototype

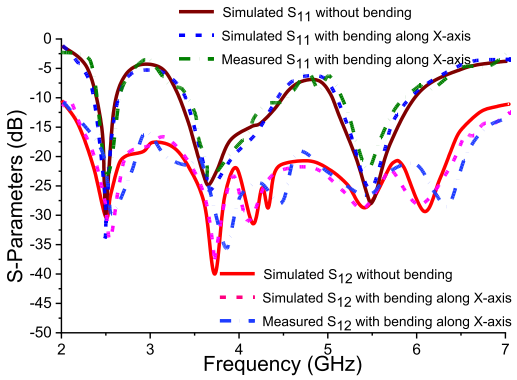

(c) S-Parameter

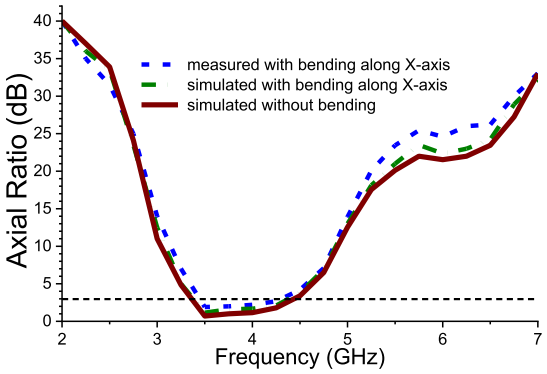

(d) AR

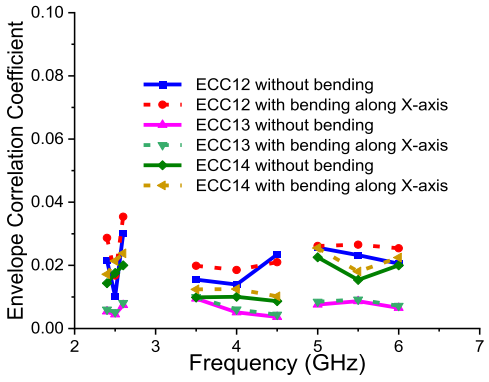

(e) ECC

FIGURE 25. **Bending analysis along X-axis.**

small decrease in the bandwidth and minor shift in frequency, it can still cover the entire 5 GHz WLAN band. The simulated and measured transmission coefficient of the bending MIMO antenna is well below -20 dB throughout the three operating bands, and they conform well with the simulation results of the one without bending. From Figures 26d-e, a negligible deviation in the AR and ECC curves is observed, and they are acceptable within the required range.

VII. PERFORMANCE COMPARISON OF PROPOSED FLEXIBLE FOUR PORT DUAL CP MIMO ANTENNA

In order to validate the novelty and suitability of the proposed decagon shaped dual polarized flexible MIMO antenna, it is compared with the existing state of art as shown in Table 3.

From the above table it can be concluded that the proposed decagon shaped dual polarized MIMO antenna is smallest in size as compared to all the reported state of arts, covers multiple bands as compared to [5], [7], [10], [16], [18], [21], and [22] is cost-effective as compared to [6], [7], [18], and [26] as well as uses low-cost flexible substrate apart from [1] and [22]. Thus, the proposed decagon shaped dual polarized flexible MIMO antenna is novel is design with multiple bands, compact in size, cost-effective, easy to manufacture and is thus a suitable for small form factor next-generation wireless devices.

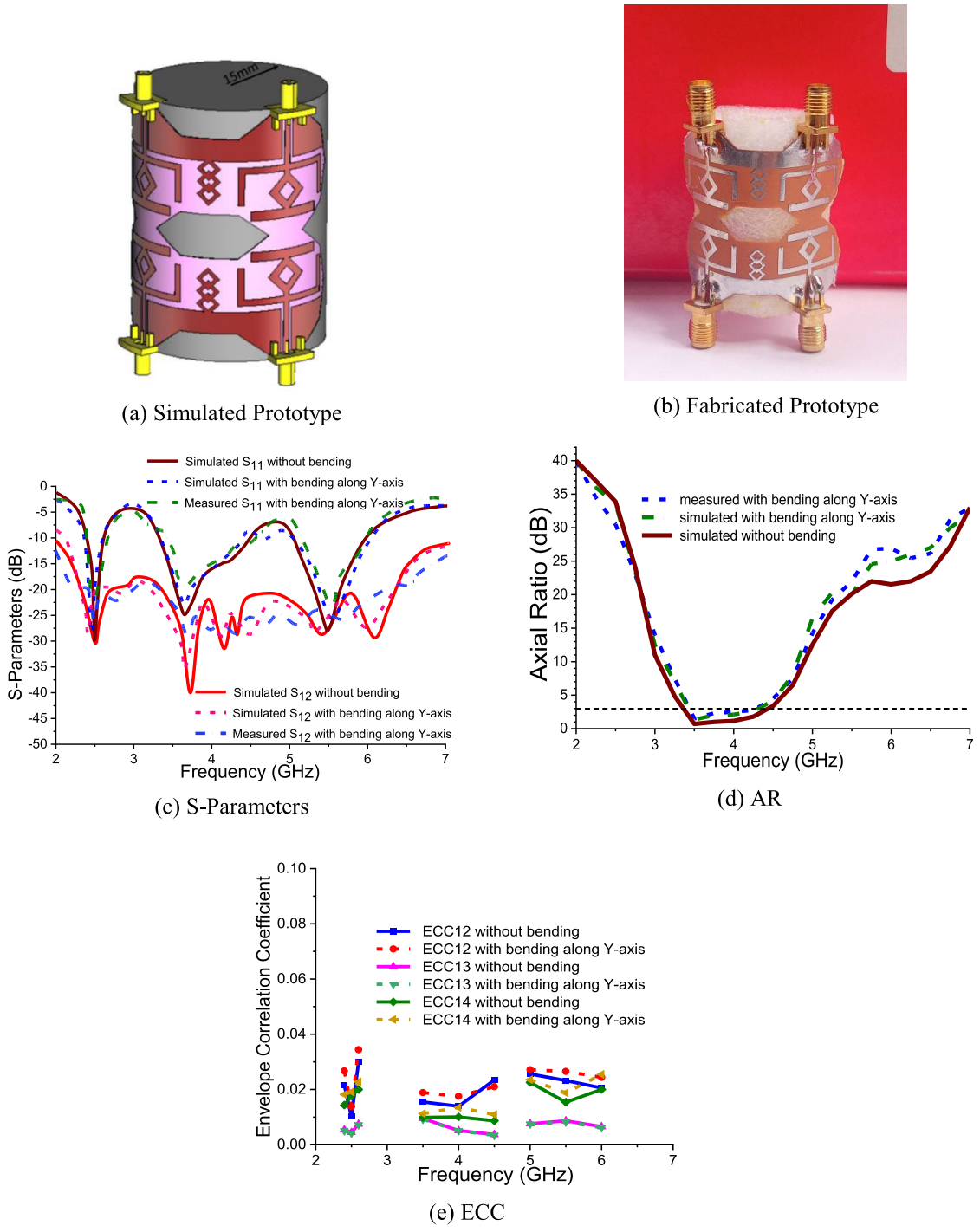

FIGURE 26. **Bending analysis along Y-axis.**

VIII. CONCLUSION

A very low-profile decagon shaped dual polarized flexible MIMO antenna with pattern diversity has been successfully studied. The proposed flexible MIMO antenna is cost-effective, easy to design, occupies a volume size of $1.896 \times 10^{-4}\lambda^3$, and operates at LTE 38/40, 5G Sub-6 GHz NR band n77/n78, and WLAN/Wi-Fi frequency bands for next-generation wireless devices. Due to the bevelled ground plane embedded on the decagon shaped substrate and the small diamond-shaped ring radiator protruding from the U-shaped radiator, desired CP bandwidth of 28.79% (3.30–4.41 GHz) was excited across the Sub-6 GHz frequency band. Furthermore, the proposed flexible MIMO antenna has exhibited good radiation characteristics with

nearly omnidirectional radiation patterns, gain larger than 4 dBi with nearly and stable efficiency above 80% across the three desired bands of interest. From the bending analysis performed on the proposed flexible MIMO antenna, desirable performances in terms of scattering parameters, 3 dB ARBW, and ECC are demonstrated with very minor detrimental effects. The above characteristics make the proposed flexible MIMO antenna a suitable candidate for small form factor next-generation wireless devices.

REFERENCES

[1] A. Omar, M. Hussein, I. J. Rajmohan, and K. Bathich, "Dual-band MIMO coplanar waveguide-fed-slot antenna for 5G communications," *Heliyon*, vol. 7, pp. 1–10, Apr. 2021.

[2] J. Kulkarni, A. Desai, and C. Y. D. Sim, "Wideband four-port MIMO antenna array with high isolation for future wireless systems," *Int. J. Electron. Commun.*, vol. 128, pp. 1–14, Jan. 2021.

[3] K. R. Jha, Z. A. P. Jibran, C. Singh, and S. K. Sharma, "4-port MIMO antenna using common radiator on a flexible substrate for sub-1 GHz, sub-6 GHz 5G NR, and Wi-Fi 6 applications," *IEEE Open J. Antennas Propag.*, vol. 2, pp. 689–701, 2021.

[4] S. Saxena, B. K. Kanaujia, S. Dwari, S. Kumar, and R. Tiwari, "MIMO antenna with built-in circular shaped isolator for sub-6 GHz 5G applications," *Electron. Lett.*, vol. 54, pp. 1–2, Apr. 2018.

[5] J. Su, Z. Dai, J. Du, J. Yu, Z. Chen, and Z. Li, "A compact dual-band MIMO antenna for 5G mobile communications," *ACES J.*, vol. 34, no. 11, pp. 1731–1738, Nov. 2019.

[6] H. H. Tran, N. Hussain, and T. T. Le, "Low-profile wideband circularly polarized MIMO antenna with polarization diversity for WLAN applications," *AEU-Int. J. Electron. Commun.*, vol. 108, pp. 172–180, Aug. 2019.

[7] M. Y. Jamal, M. Li, and K. L. Yeung, "Isolation enhancement of closely packed dual circularly polarized MIMO antenna using hybrid technique," *IEEE Access*, vol. 8, pp. 11241–11247, 2020.

[8] U. Ullah, I. B. Mabrouk, and S. Koziel, "Enhanced-performance circularly polarized MIMO antenna with polarization/pattern diversity," *IEEE Access*, vol. 8, pp. 11887–11895, 2020.

[9] Q. Luo, S. Gao, and L. Zhang, "Wideband multilayer dual circularly-polarized antenna for array application," *Electron. Lett.*, vol. 51, pp. 2087–2088, Dec. 2015.

[10] S. Chaudhuri, R. S. Kshetrimayum, and R. K. Sonkar, "High inter-port isolation dual circularly polarized slot antenna with split-ring resonator based novel metasurface," *AEU-Int. J. Electron. Commun.*, vol. 107, pp. 146–156, Jul. 2019.

[11] H. Arun, "CPW fed circularly polarized wideband pie-shaped monopole antenna for multi-antenna techniques," *COMPEL-Int. J. Comput. Math. Electr. Electron. Eng.*, vol. 37, no. 6, pp. 2109–2121, Nov. 2018.

[12] I. Adam, M. N. M. Yasin, N. Ramli, M. Jusoh, H. A. Rahim, T. B. A. Latef, T. F. T. M. N. Izam, and T. Sabapathy, "Mutual coupling reduction of a wideband circularly polarized microstrip MIMO antenna," *IEEE Access*, vol. 7, pp. 97838–97845, 2019.

[13] L. Malviya, R. K. Panigrahi, and M. V. Kartikeyan, "Circularly polarized 2 × 2 MIMO antenna for WLAN applications," *Prog. Electromagn. Res. C*, vol. 66, pp. 97–107, 2016.

[14] R. Subhanrao Bhadade and S. Padmakar Mahajan, "'Circularly polarized 4 × 4 MIMO antenna for WLAN application,'" *Electromagnetics*, vol. 39, no. 5, pp. 325–342, Jul. 2019.

[15] E. Zhang, A. Michel, M. R. Pino, P. Nepa, and J. Qiu, "A dual circularly polarized patch antenna with high isolation for MIMO WLAN applications," *IEEE Access*, vol. 8, pp. 117833–117840, 2020.

[16] S. Saxena, B. K. Kanaujia, S. Dwari, S. Kumar, H. C. Choi, and K. W. Kim, "Planar four-port dual circularly-polarized MIMO antenna for sub-6 GHz band," *IEEE Access*, vol. 8, pp. 90779–90791, 2020.

[17] S. Kumar, G. H. Lee, D. H. Kim, H. C. Choi, and K. W. Kim, "Dual circularly polarized planar four-port MIMO antenna with wide axial-ratio bandwidth," *Sensors*, vol. 20, no. 19, p. 5610, Sep. 2020.

[18] S. S. Singhwal, B. K. Kanaujia, A. Singh, J. Kishor, and L. Matekovits, "Multiple input multiple output dielectric resonator antenna with circular polarized adaptability for 5G applications," *J. Electromagn. Waves Appl.*, vol. 34, no. 9, pp. 1180–1194, Feb. 2020.

[19] H. N. Chen, J.-M. Song, and J.-D. Park, "A compact circularly polarized MIMO dielectric resonator antenna over electromagnetic band-gap surface for 5G applications," *IEEE Access*, vol. 7, pp. 140889–140898, 2019.

[20] A. Altaf and M. Seo, "Size-reduction of a dual-band circularly polarized dielectric resonator antennas," *IEEE Access*, vol. 9, pp. 126457–126465, 2021.

[21] N. K. Sahu, G. Das, and R. K. Gangwar, "Circularly polarized offset-fed DRA elements & their application in compact MIMO antenna," *Eng. Sci. Technol., Int. J.*, vol. 28, Apr. 2022, Art. no. 101015.

[22] G. Varshney, R. Singh, V. S. Pandey, and R. S. Yaduvanshi, "Circularly polarized two-port MIMO dielectric resonator antenna," *Prog. Electromagn. Res. M*, vol. 91, pp. 19–28, 2020.

[23] J. Iqbal, U. Illahi, M. I. Sulaiman, M. M. Alam, M. M. Su'ud, and M. N. M. Yasin, "Mutual coupling reduction using hybrid technique in wideband circularly polarized MIMO antenna for WiMAX applications," *IEEE Access*, vol. 7, pp. 40951–40958, 2019.

[24] S. G. Kirtania, A. W. Elger, M. R. Hasan, A. Wisniewska, K. Sekhar, T. Karacolak, and P. K. Sekhar, "Flexible antennas: A review," *Micromachines*, vol. 11, no. 9, p. 847, Sep. 2020.

[25] W. Li, Y. Hei, P. M. Grubb, X. Shi, and R. T. Chen, "Compact inkjet-printed flexible MIMO antenna for UWB applications," *IEEE Access*, vol. 6, pp. 50290–50298, 2018.

[26] C. Du, X. Wang, and G.-Y. Jin, "A compact tri-band flexible MIMO antenna based on liquid crystal polymer for wearable applications," *Prog. Electromagn. Res. M*, vol. 102, pp. 217–232, 2021.

[27] H. Li, S. Sun, B. Wang, and F. Wu, "Design of compact single-layer textile MIMO antenna for wearable applications," *IEEE Trans. Antennas Propag.*, vol. 66, no. 6, pp. 3136–3141, Jun. 2018.

[28] S. M. Saeed, C. A. Balanis, and C. R. Birtcher, "Flexible reconfigurable antenna with MIMO configuration," in *Proc. IEEE Int. Symp. Antennas Propag. USNC/URSI Nat. Radio Sci. Meeting*, Jul. 2017, pp. 1643–1644.

[29] C. A. Balanis, *Antenna Theory Analysis and Design*, 3rd ed. Hoboken, NJ, USA: Wiley, 2005.

[30] J. Kulkarni, A. Desai, and C. Sim, "Two port CPW-fed MIMO antenna with wide bandwidth and high isolation for future wireless applications," *Int. J. RF Microw. Comput.-Aided Eng.*, vol. 31, no. 8, pp. 1–18, Aug. 2021.

[31] A. G. Alharbi, J. Kulkarni, A. Desai, C.-Y.-D. Sim, and A. Poddar, "A multi-slot two-antenna MIMO with high isolation for sub-6 GHz 5G/IEEE802.11 ac/ax/C-band/X-band wireless and satellite applications," *Electronics*, vol. 11, no. 3, p. 473, Feb. 2022, doi: 10.3390/electronics11030473.

[32] J. Kulkarni, C.-Y.-D. Sim, A. Desai, E. Holdengreber, R. Talware, V. Deshpande, and T. K. Nguyen, "A compact four port ground-coupled CPWG-fed MIMO antenna for wireless applications," *Arabian J. Sci. Eng.*, vol. 47, no. 11, pp. 14087–14103, Nov. 2022, doi: 10.1007/s13369-022-06620-z.

[33] M. Ameen, O. Ahmad, and R. K. Chaudhary, "Wideband circularly-polarised high-gain diversity antenna loaded with metasurface reflector for small satellite applications," *Electron. Lett.*, vol. 55, no. 15, pp. 829–831, Jul. 2019.

[34] M. Ameen, O. Ahmad, and R. K. Chaudhary, "Bandwidth and gain enhancement of triple-band MIMO antenna incorporating metasurface-based reflector for WLAN/WiMAX applications," *IET Microw., Antennas Propag.*, vol. 14, no. 13, pp. 1493–1503, Oct. 2020.

[35] M. Ameen, T. Prakash, and R. K. Chaudhary, "Eight-port octagonal-shaped metasurface-based MIMO antenna with radar cross section reduction," in *IEEE MTT-S Int. Microw. Symp. Dig.*, Dec. 2021, pp. 17–19.

[36] A. Kumar, A. A. Althuwayb, D. Chaturvedi, R. Kumar, and F. Ahmadfard, "Compact planar magneto-electric dipole-like circularly polarized antenna," *IET Commun.*, vol. 16, no. 20, pp. 2448–2453, Dec. 2022.

[37] R. Kumar, S. R. Thummaluru, and R. K. Chaudhary, "Improvements in Wi-MAX reception: A new dual-mode wideband circularly polarized dielectric resonator antenna," *IEEE Antennas Propag. Mag.*, vol. 61, no. 1, pp. 41–49, Feb. 2019, doi: 10.1109/MAP.2018.2883013.

[38] A. Chandra, N. Mishra, R. Kumar, K. Kumar, and H. Y. Patil, "A superstrate and FSS embedded dual band waveguide aperture array with improved far-field characteristics," *Microw. Opt. Technol. Lett.*, vol. 2022, pp. 1–7, Oct. 2022, doi: 10.1002/mop.33492.

JAYSHRI KULKARNI (Senior Member, IEEE) received the B.E. degree in electronics and tele-communication engineering from Shivaji University, Maharashtra, India, in 2005, the M.E. degree in microwave engineering from the PICT College, Pune, Maharashtra, in 2011, and the Ph.D. degree in electronics and communication engineering from Anna University, Chennai, India, in 2020. From 2006 to 2009, she was a Lecturer with the Genba Sopanrao Moze College of Engineering, Pune, and from 2010 to 2022, she was as an Assistant Professor with the Department of Electronics and Telecommunication Engineering, Vishwakarma Institute of Information Technology, Pune. She is currently working as a Postdoctoral Research Associate with Baylor University, Waco, TX, USA. She has authored more than ten books and more than 50 research articles in reputed journals and conferences. Her research interests include antennas, microwave engineering, wireless communication, and wireless sensor networks. Her awards include Desmond Sim Award for the Best Antenna Design Paper at IEEE InCAP 2019, India; the Outstanding Oral Presentation Award at ICRAMET-2020, Indonesia; and the Best Paper of the Session Award at IEEE ESCI-2021, Pune. She was one of the recipient of Mojgan Daneshmand Grant awarded by IEEE Antennas and Propagation Society (AP-S)-2022. She is also serving as a Vice-Chair for the Joint Chapter of APS/MTT/EMC, Pune Chapter.

ABDULLAH G. ALHARBI (Member, IEEE) received the B.Sc. degree in electronics and communications engineering from Qassim University, Saudi Arabia, in 2010, and the master's and Ph.D. degrees in electrical engineering from the University of Missouri Kansas City, USA, in 2014 and 2017, respectively. From 2010 to 2012, he was an Electrical Engineer with Saudi Aramco Company. He is currently an Assistant Professor with the Department of Electrical Engineering, Jouf University, Saudi Arabia. He authored or coauthored over 45 journals and conference papers and one Springer book. His research interests include digital IC design, memristor-based circuits, nanoelectronics, network routing, green communications, and wireless communications. He is a member of the Gulf Engineering Union, the IEEE Circuits and Systems Society, the IEEE Young Professionals, the IEEE Signal Processing Society, the IEEE Instrumentation and Measurement Society Membership, and the IEEE Communications Society Membership, and a Professional Member of ACM. He was a recipient of several awards from Saudi Arabian Cultural Mission, USA, and the University of Missouri Kansas City.

CHOW-YEN-DESMOND SIM (Senior Member, IEEE) was born in Singapore, in 1971. He received the B.Sc. degree from the Department of Engineering, University of Leicester, U.K., in 1998, and the Ph.D. degree from the Radio System Group, Department of Engineering, University of Leicester, in 2003. From 2003 to 2007, he was an Assistant Professor with the Department of Computer and Communication Engineering, Chienkuo Technology University, Changhua, Taiwan. In 2007, he joined the Department of Electrical Engineering, Feng Chia University (FCU), Taichung, Taiwan, as an Associate Professor, where he became a Full Professor, in 2012, and as a Distinguish Professor, in 2017. He worked as the Executive Officer of Master's Program with the College of Information and Electrical Engineering (Industrial Research and Development) and the Director of the Intelligent IoT Industrial Ph.D. Program, from August 2015 to July 2018. He co-founded the Antennas and Microwave Circuits Innovation Research Center, FCU, and worked as the Director, from 2016 to 2019. Since October 2016, he has been serving as the Technical Consultant for Securitag Assembly Group (SAG), which is one of the largest RFID tag manufacturers in Taiwan. He has been serving as the Consultant for Avary (the largest PCB manufacturer in mainland China), since August 2018. He worked as the Head of the Department of Electrical Engineering, FCU, from August 2018 to July 2021. He has authored or coauthored over 180 SCI articles. His current research interests include antenna design, VHF/UHF tropospheric propagation, and RFID applications. He is a fellow of the Institute of Engineering and Technology (FIET), a Senior Member of the IEEE Antennas and Propagation Society, and a Life Member of the IAET. He has served as the TPC member for many international conferences. He was a recipient of the IEEE Antennas and Propagation Society Outstanding Reviewer Award IEEE TRANSACTIONS ON ANTENNAS AND PROPAGATION, for eight consecutive years, from 2014 to 2021. He has also received the Outstanding Associate Editor Award from the IEEE ANTENNAS WIRELESS AND PROPAGATION LETTERS, in July 2018. He has served as the TPC Sub-Committee Chair (Antenna) for the ISAP 2014 and PIERS 2017/2019. He has served as the Advisory Committee for InCAP 2018/2019 and ICoICCS 2021, and has also served as the TPC Chair for the APCAP 2016 and iWEM 2019/2020, and the Track Chair for ICCC 2022. He was the General Co-Chair of ISAP 2021. He has served as the Chapter Chair for the IEEE AP-Society, Taipei Chapter, from January 2016 to December 2017. He was the Founding Chapter Chair of the IEEE Council of RFID, Taipei Chapter, from October 2017 to December 2020. He was invited as the Workshop/Tutorial Speaker of APEMC 2015, iAIM 2017, and InCAP 2018, and the Invited Speaker of TDAT 2015, iWAT 2018, APCAP 2018, ISAP 2019, InCAP 2019, ISRAST 2020, ISAP 2020, URSI GASS 2021, iWEM 2021, WAMS 2022, and ISAP 2022. He was the Keynote Speaker of SOLI 2018 and NEAST 2020. He has served as the Associate Editor for IEEE ACCESS, from August 2016 to January 2021. He is also serving as an Associate Editor for the IEEE ANTENNAS AND WIRELESS PROPAGATION LETTERS, the IEEE JOURNAL OF RADIO FREQUENCY IDENTIFICATION, and *International Journal of RF and Microwave Computer-Aided Engineering* (Wiley).

ISSA ELFERGANI (Senior Member, IEEE) received the M.Sc. and Ph.D. degrees in electrical and electronic engineering from the University of Bradford, U.K., in 2008 and 2013, respectively. After his Ph.D. degree, since 2013, he has been working as a Postdoctoral Researcher and then as an Investigator Junior at the Mobile Systems Group, Instituto de Telecomunicações, Aveiro, Portugal. In 2014, he received prestigious FCT Fellowship for his postdoctoral research. The evaluation of the first triennium of this scholarship was given an excellent rating by the evaluators. He is currently a Senior Researcher with the Instituto de Telecomunicações, working with European research-funded projects, while leading technical activities in antenna design for ENIAC ARTEMOS (2011–2014), EUREKA BENEFIC (2014–2017), CORTIF (2014–2017), GREEN-T (2011–2014), VALUE (2016–2016), THINGS2DO (2014–2018), H2020-ITN-SECRET (2017–2020), POSITION-II (2018-2021), and Moore4Medical (2019–2023), some of projects have been successfully concluded and some still ongoing. He is also working on (5GWAR) Novel 5G Millimetre-Wave Array Antennas for Future Mobile Handset Applications as a Principle Investigator. He is also an Honorary Visiting Research Fellow with the Faculty of Engineering and Informatics, University of Bradford, U.K. He has around 160 high-impact publications in international conferences, journal papers, and book/book chapters with a Google scholar H-index 21. He is a member of IET. He is the Guest Editor/Special Issue of Electronics Recent Technical Developments in Energy Efficient 5G Mobile Cells and Special Issue on Recent Advances in Engineering Systems Journal (ASTESJ), a Guest Editor/Special Issue of Electronics Recent Advances in Antenna Design for 5G Heterogeneous Networks, and a Guest Editor/Special Issue of Electronics "Unable RF Front-End Circuits for 5G and Beyond: Design, Challenges and Applications."

JAUME ANGUERA (Fellow, IEEE) was born in Vinaròs, Spain, in 1972. He received the Technical Engineering degree (three years degree) in electronic systems and the Engineering degree (five years degree) in electronic engineering from Ramon Llull University (URL), Barcelona, Spain, in 1994 and 1998, respectively, and the Telecommunication Engineering degree (five years degree) and the Ph.D. degree in telecommunications from the Polytechnic University of Catalonia (UPC), Barcelona, in 1998 and 2003, respectively.

He is currently the Founder and a CTO with Ignion, and an Associate Professor with Universitat Ramon LLull, all institutions in Barcelona. From 1997 to 1999, he joined the Electromagnetic and Photonic Engineering Group, Signal Theory and Communications Department, UPC, as a Researcher in microstrip fractal-shaped antennas. In 1999, he was a Researcher at Sistemas Radiantes, Madrid, Spain, where he was involved in designing dual-band dual-polarized fractal-inspired microstrip patch arrays for mobile communications. In the same year 1999, he became an Assistant Professor at the Department of Electronics and Telecommunications, Universitat Ramon Llull-Barcelona, and an Associate Professor, in 2016, where he is currently teaching antenna theory. Since 2001, he has led research projects in the antenna field for wireless applications in a frame of industry-university collaboration: Ignion and the Department of Electronics and Telecommunications, Universitat Ramon Llull-Barcelona. Several of his supervised students have been awarded Best Bachelor's and Master's Thesis by the Spanish Ministry and other Spanish institutions. From 1999 to 2017, he was with Fractus (founder partner), Barcelona, where he held the position of a research and development manager and developed various cutting-edge antenna technologies. At Fractus, he led projects on antennas for base station systems antennas for automotive. From 2003 to 2006, he was also assigned to Fractus in South Korea to head up the research team. One of his main tasks was to provide training, education, and development of the team's core competency and provide a research and development vision to address the rapidly growing mobile device market. Under his leadership, the company had secured major contracts with companies, such as Samsung, LG, and Bellwave, to name a few. He published a book about "Korean Experiences," in 2015. Since 2017, he has been with Ignion in the role of CTO. He leads the company's research and development activity to create new products, envisage new technologies and technical evangelism, foster synergies with partners, and provide technology strategy to scale the company's business. He holds more than 150 granted invention patents (USA, Asia, and Europe) in the antenna field, many of which have been licensed to antenna companies. Among his most outstanding contributions is that of the inventor of antenna booster technology, a technology that fostered the creation of Ignion. The wireless industry has adopted many of these products worldwide to allow wireless connectivity to the IoT devices through a miniature component called an antenna booster that is ten times smaller than conventional antennas. He is the author of more than 270 journals and international and national conference papers (H-index=52 with more than 8000 citations based on Google-Scholar). He has taught more than 50 antenna courses worldwide (USA, China, South Korea, India, U.K., France, Poland, Czech Republic, Tunisia, Perú, Brazil, Canada, and Spain). He has directed over 150 bachelor's, master's, and Ph.D. theses. He has authored seven books. He has participated in over 20 national/international projects and research grants valued at over €13 million, of which he was the principal researcher in many of them. His current research interests include antenna boosters, multiband and small antennas, broadband matching networks, diversity antenna systems/MIMO, electromagnetic dosimetry, genetically optimised antennas, and antennas for wireless handset devices.

Dr. Anguera was a member of the fractal team that in 1998 received the European Information Technology Grand Prize for the Applied Science and Engineering for the fractal-shaped antenna application to cellular telephony. He was a 2003 Finalist for the Best Doctoral Thesis on UMTS (Fractal and Broadband Techniques on Miniature, Multifrequency, and High-Directivity Microstrip Patch Antennas); prize promoted by "Technology Plan of UMTS Promotion" given by Telefónica Móviles España) and New faces of Engineering 2004 (promoted by IEEE and IEEE Foundation). In the same year, he won the Best Doctoral Thesis (Ph.D.) in "Network and Broadband Services" (XXIV Prize Edition "Ingenieros de Telecomunicación") organized by Colegio Oficial de Ingenieros de Telecomunicación (COIT) and the Company ONO (National Price). In 2011, he received the Alè Vinarossenc recognition by Fundació Caixa Vinaròs. In 2014, together with four other Fractus inventors, he received the "2014 Finalist to European Patent Award." He is Vice-Chair of the Working Group "Software and Modeling" with EurAAP. He is a reviewer for several IEEE journals as well as others. He is an Associate with IEEE Open Journal on Antennas and Propagation and *Electronics Letters*. His biography is listed in Who'sWho in the World, Who'sWho in Science and Engineering, Who'sWho in Emerging Leaders, and International Biographical Center (IBC), Cambridge, U.K. He is an IEEE Antennas and Propagation Distinguished Lecturer. His detailed information can be found at: http://users.salleurl.edu/~jaume.anguera

CHEMSEDDINE ZEBIRI (Senior Member, IEEE) received the degree in electronics engineering from the University of Constantine, Algeria, in 2001, the Magister degree from the University of Ferhat Abbas, Sétif, Algeria, in 2003, and the Ph.D. degree in electronics from the University of Constantine, in 2011. In 2006, he was a Senior Lecturer with the Department of Electronics, University of Ferhat Abbas, where he is currently an Associate Professor. He has published up to 100 journal articles and refereed conference papers. His current research interests include dielectric resonator antennas, MIMO antennas, mmWave antennas, magnetic materials, complex material components in the microwaves, and optical domains.

JONATHAN RODRIGUEZ (Senior Member, IEEE) received the master's and Ph.D. degrees in electronic and electrical engineering from the University of Surrey, U.K., in 1998 and 2004, respectively. In 2005, he became a Researcher at the Instituto de Telecomunicações, Portugal. In 2017, he was appointed as a Professor of mobile communications at the University of South Wales, U.K. He has served as a Project Co-ordinator for major international research projects, including Eureka LOOP, FP7 C2POWER, and H2020-SECRET, whilst serving as a Technical Manager for FP7 COGEU and FP7 SALUS. He is the author of more than 500 scientific works, including 11 book editorials. He is a fellow of the IET (FIET) and a Senior Fellow of the Higher Education Academy (SFHEA). His professional affiliations include Chartered Engineer (C.Eng.).